Oil & Natural Gas Technology

DOE Award No.: DE-FC26-06NT42664

Semi-Annual Report

GEOMECHANICAL PERFORMANCE OF HYDRATE-BEARING SEDIMENTS IN OFFSHORE ENVIRONMENTS

Submitted by:
Texas A&M University
507 Richardson Building
College Station, Texas 77843

Prepared for:
United States Department of Energy
National Energy Technology Laboratory

October, 2007

Office of Fossil Energy

TABLE OF CONTENTS

List of Figures

List of Tables

1. Executive Summary

The objective of this multi-year, multi-institutional research project is to develop the knowledge base and quantitative predictive capability for the description of geomechanical performance of hydrate-bearing sediments (hereafter referred to as HBS) in oceanic environments. The focus is on the determination of the envelope of hydrate stability under conditions typical of those related to the construction and operation of offshore platforms. We have developed a robust numerical simulator of hydrate behavior in geologic media by coupling a reservoir model with a commercial geomechanical code. We are also investigating the geomechanical behavior of oceanic HBS using pore-scale models (conceptual and mathematical) of fluid flow, stress analysis, and damage propagation.

We are using data from the literature and we are conducting laboratory studies to generate data to (i) evaluate the conceptual pore-scale models, (ii) calibrate the mathematical models, (iii) determine dominant relations and critical parameters defining the geomechanical behavior of HBS, and (iv) establish relationships between the geomechanical status of HBS and the corresponding geophysical signature. Four organizations, Texas A&M University (TAMU), University of California at Berkeley (UCB), Lawrence Berkeley National Laboratory (LBNL), and Schlumberger (SLB), who are involved in this project..

Pore Scale Modeling by UCB

The objective of the UC Berkeley work is to develop a grain-scale model of hydrate-bearing sediments. Hydrate dissociation alters the strength of HBS. In particular, transformation of hydrate clusters into gas and liquid water weakens the skeleton and, simultaneously, reduces the effective stress by increasing the pore pressure. The large-scale objective of the study is evaluation of geomechanical stability of offshore oil and gas production infrastructure. The output of the micro-scale model described here will be used in the numerical simulations of coupled flow and rock mechanics at reservoir scale.

We model the mechanical deformation of HBS or, more generally, of a granular medium, by numerical simulations of a pack of elastic spherical grains. Although this approach cannot entirely displace laboratory tests as the ground truth, it offers some opportunities which may be not available otherwise. Grain-scale simulations provide unique insights into the processes and phenomena underlying the classical continuum-medium models. For example, such simulations provide a physical explanation and quantitative assessment of strain hardening and irreversibility. Various what-if scenarios, which cannot be performed in a laboratory, can be played on numerical models at practically zero cost.

Summary of TOUGH+/FLAC3D Model Development by LBNL

In the second half of FY 2007, Lawrence Berkeley National Laboratory researchers 1) submitted a topical report entitled "Approach to Forming Hydrate Bearing Samples in Fine-Grained Material", 2) designed and completed fabrication of a geomechanical properties and geophysical signature test cell, 3) tested seismic transducers to be used in the test cell, and 4) attended and made two presentations at the DOE Program Review.

The topical report entitled "Approach to Forming Hydrate Bearing Samples in Fine-Grained Material", summarized methods to make methane hydrate for the geomechanical tests to be performed, in the types of sediments recommended by Texas A&M University. These sediments were described as (1) 100% sand sized particles (100 microns), (2) 50% silt-sized particles (10 microns) mixed with 50% clay-sized particles (1 micron), and (3)100% clay sized particles.

The method proposed follows these steps and the method was accepted by DOE in July, 2007.

- Mix dry mineral components until visually homogeneous
- Add water using a pipette (for sand), by equilibrating in a humidified chamber (silt or clay), or by stirring in flakes of frost ice (samples containing clay) and mix thoroughly
- Pack moistened material into the sleeve
- Rapidly evacuate air from the sample
- Chill sample to the appropriate temperature
- Pressurize sample with methane gas, and monitor T, P until hydrate is formed.
- Saturate with water

Simulation of Gas Production from Hydrates Using TOUGH+Hydrate by TAMU

To simulate geomechanical stability in subsea hydrate bearing sediments, it is important to understand the fundamental concepts of gas production from gas hydrates or free gas zones beneath gas hydrates. The flow of gas and water are inherently coupled with the mechanical properties of the hydrate bearing sediments. To model a field scale geomechanical failure or response, one should clearly understand the field scale flow concepts in a hydrate bearing sediment.

Now that **TOUGH+Hydate** contains the FLAC3D model as a subroutine, we are ready to begin simulation work to investigate how gas production from gas hydrate zones affects the formation mechanical properties and seafloor slope stability. To be certain we are simulating the gas flow from gas hydrate deposits correctly, we have chosen to use **TOUGH+Hydate** to analyze data from the one known gas hydrate field that has been produced. As such, we have used the **TOUGH+Hydrate** simulator to reproduce some important observations and pressure behavior at Messoyakha. Through our modeling study of Messoyakha, we evaluated different reservoir/rock properties which are important for response of hydrate bearing sediments/rocks. This study has actually helped us understand how to accurately model flow in hydrate bearing sediment.

We have used **TOUGH+Hydrate** to simulate the observed gas production and reservoir pressure field data at Messoyakha. We simulated various scenarios that help to explain the field behavior. We have evaluated the effect of various reservoir parameters on gas recovery from hydrates. Our work should be beneficial to others who are investigating how to produce gas from hydrate capped gas reservoir. We were able to generate results that are very similar to the reported flow rates and pressure behavior in the Messoyakha Field. The value of absolute permeability in the hydrate layer and the lower free gas layer substantially affects the continued dissociation of hydrates during shut-down. We also modeled the formation of secondary hydrates near the wellbore that can cause reduced gas flow rates. The important parameters affecting the gas production are the formation permeability in the gas layer, the effective gas vertical permeability in the hydrate layer, the location of the perforations, and the gas hydrate saturation.

Summary of Petrel-FLAC3D Data Exchange by Schlumberger

The PETREL model contains, among other things, the description of horizons and the special distribution of properties. As part of this project, an automatic method of creating a FLAC3D grid must be developed. The resulting grid must be composed of multiple materials representing the various regions of the PETREL database delimited by the horizons.

In addition to the grid, an automatic and conservative method of extracting material properties from PETREL should also be devised. The extracted properties should be automatically assigned to the individual FLAC3D grid element. The user will complement the missing material properties and mechanical behavior law parameters by adding them manually to the FLAC3D data file.

A number of comments are in order

1. Data sets extracted from PETREL may be very large. An automatic method should be devised to coarsen (decimate) the data, while maintaining pertinent details.
2. The PETREL model may contain features ranging in size from tens of meters to hundreds of kilometers. This requires a non-traditional meshing approach that would keep the total element count in the FLAC3D model to a minimum while ensuring adequate representation of details and adequate transition between FLAC3D element sizes.
3. Property transfer from PETREL to FLAC3D should be conservative
4. The workflow should be simple and robust

2. Introduction

Gas hydrate is a solid material resulting from the orderly assembly of gas molecules such as methane, carbon dioxide, and hydrogen sulfide, within a clathrate (cage like) structure of water molecules under moderate (relative to conventional oil and gas reservoir conditions) pressure and temperature. Vast amounts of hydrocarbons are trapped in hydrate deposits (Sloan, 1998). Such deposits occur in two distinctly different geologic settings where the necessary low temperatures and high pressures exist for their formation and stability: in the permafrost and in deep ocean sediments near the sea floor.

The three main methods of hydrate dissociation are (1) depressurization, in which the pressure is lowered to a level lower than the hydration pressure P_H at the prevailing temperature, (2) thermal stimulation, in which the temperature is raised above the hydration temperature T_H at the prevailing pressure, and (3) the use of inhibitors (such as salts and alcohols), which causes a shift in the P_H-T_H equilibrium through competition with the hydrate for guest and host molecules (Sloan, 1998). Dissociation results in the production of gas and water, with a commensurate reduction in the saturation of the solid hydrate phase.

Gas hydrates exist in many configurations below the sea floor including massive (thick solid zones), continuous layers, nodular, and disseminated occurrences each of which may affect the seafloor stability differently. The hydrates in all of these configurations may be part of the solid skeleton that supports overlying sediments, which ultimately support platforms and pipelines needed for production from conventional oil and gas resources, and from the eventual production from hydrate accumulations.

During dissociation, the basal zone of the gas hydrate becomes under-consolidated and possibly over-pressured because of the newly released gas (Schmuck and Paull, 1993), leading to a zone of weakness (i.e., low shear strength, where failure could be triggered by gravitational loading or seismic disturbances) that can ultimately result in submarine landslides (McIver, 1977; Paull et al., 1996). Possible mechanisms that can induce dissociation in Hydrate-Bearing Sediments (hereafter referred to as HBS) include an increase in salinity, a drop in the sea level and an increase in the sediment temperature (e.g., by warmer ocean bottom water, or by non-insulated pipes conducting fluids produced from deeper and warmer reservoir) can induce such dissociation.

Hydrate dissociation in HBS produces an enhanced fluidized layer at the base of the gas-hydrate zone. Submarine slope failure can follow, giving rise to debris flows, slumps, slides, and collapse depressions such as described by Dillon et al. (1998). Failure would be accompanied by the release of methane gas, but a portion of the methane is likely to be oxidized unless the gas release is catastrophic. A scenario illustrating submarine slope failure is shown in **Figure 1**. The possible connection between gas-hydrate boundaries and submarine slide and slump surfaces was first recognized by McIver (1982). Several hydrate-related occurrences of oceanic landslides are discussed in the literature. These include sediment slides and slumps on the continental slope and rise of West Africa (Summerhayes et al., 1979), slumps on the U.S. Atlantic continental slope (Carpenter, 1981), large submarine slides on the Norwegian continental margin (Evans et al., 1996; Bugge et al., 1988), sediment blocks on the sea floor in fjords of British Columbia, and massive bedding-plane slides and rotational slumps on the Alaskan Beaufort Sea continental margin (Kayen and Lee, 1993).

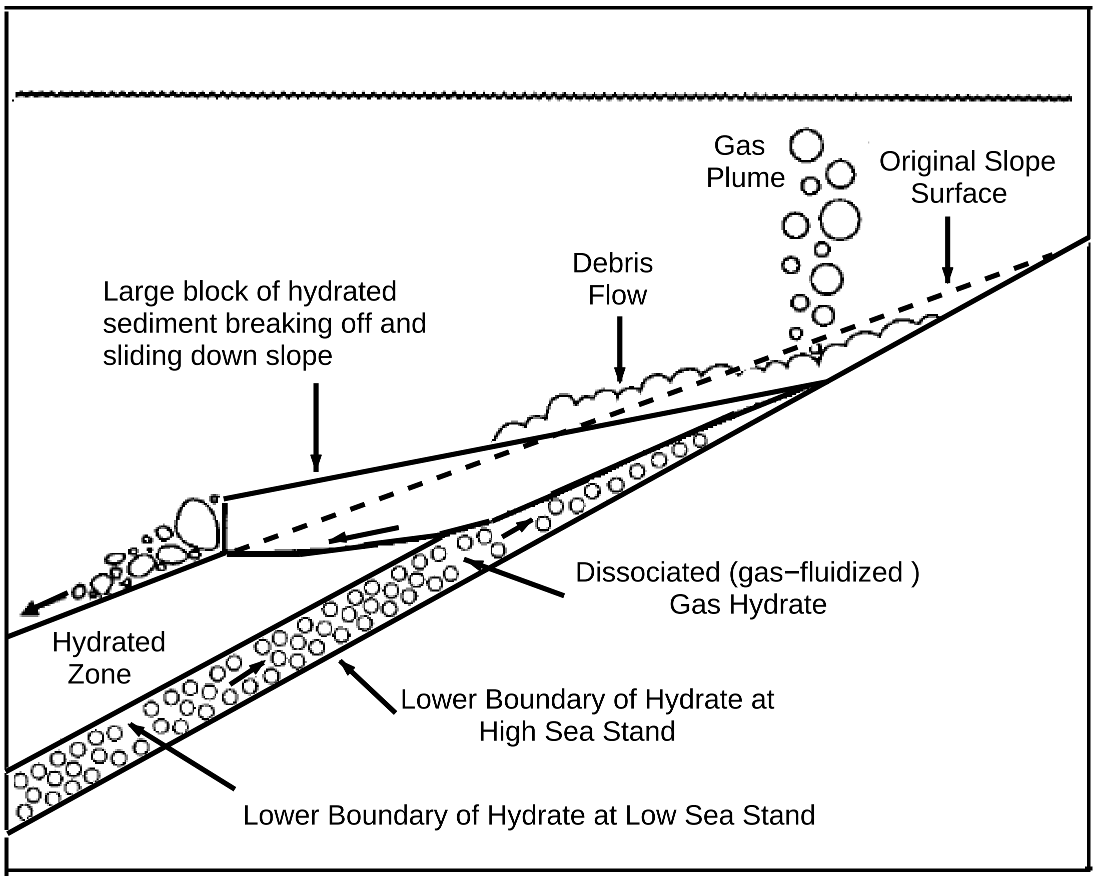

Figure 1 – Diagram showing the effects of gas hydrate dissociation on oceanic hill slope failures and gas release. Adapted from McIver (1982).

For the aforementioned stability concerns, the placement of wells and seafloor platforms associated with oil production is strongly influenced by the presence of gas hydrate on the sea floor or within the sediment lithology. These concerns will be far more pronounced if gas production from oceanic gas hydrate accumulation becomes an economically viable option. Currently, there is a lack of understanding of the mechanical and thermal properties of oceanic sediments containing gas hydrates. The general perception of instability of hydrate-bearing sediments, coupled with the lack of knowledge on the overall geomechanical behavior of such sediments, has resulted in a general strategy of avoidance of such sediments when locating offshore production platforms. By locating production platforms at sites not selected for optimum operation but dictated by the need to avoid the hydrate accumulations, the cost of production can increase significantly. Warmer oil from depth may cause gas hydrate in the neighborhood of a well or pipeline to dissociate, reducing the stability of the supports, and placing significant investments at risk. Such concerns would increase exponentially if gas is to be produced from marine hydrate accumulations, thus posing a serious impediment to the development of such resources.

Few data are available to allow one to manage the risks associated with gas hydrates on the sea floor. Understanding the thermal properties is important because heat transfer through the system is one factor that controls the rate at which the sediments are altered due to hydrate dissociation. Understanding the mechanical properties for a range of hydrate-sediment compositions will allow the prediction of stability and the management of the risks. Measurements of thermal properties have been made of mixed quartz sand and hydrate laboratory samples in addition to pure hydrate samples (Cherskii et al., 1983; Cook and Leaist, 1983; Kneafsey et al., 2005; Moridis et al., 2005a; Stoll and Bryan, 1979; Waite et al., 2002), and strength measurements have been made on laboratory-made pure methane hydrate samples (Durham et al., 2003; Stern et al., 1996). A series of measurements of mechanical, thermal, and electrical properties of tetrahydrofuran hydrate in sediment is underway (Santamarina et al., 2004). Tetrahydrofuran hydrate is stable at atmospheric pressure and near-freezing temperatures; and dissociates to tetrahydrofuran and water without the formation of a gas phase. The applicability of these measurements to the strength of gas hydrate-bearing sediments as would be found below the sea floor has yet to be established. Another study of the mechanical behavior of hydrate bearing sediments concluded that it is essential to collect more data (Hyodo et al., 2005).

The available information is not sufficient to design seafloor platforms or wells (let alone permit the design of future gas production systems from hydrates) in the vicinity of HBS considering the safety, environmental, and economic risks posed by unstable seafloor behavior. We propose to develop the necessary knowledge that will allow the determination of the envelope of safe conditions when locating and operating an offshore production platform for either conventional oil or gas production, or for production from gas hydrates. This knowledge will also provide the necessary tools to evaluate the expected stability performance of hydrate-bearing sediments, and to select optimal sites for production facility installation.

3. Technical Approach

Objective

The main objective of this multi-year research project is to develop the necessary knowledge base and quantitative predictive capability for the description of geomechanical performance of hydrate-bearing sediments (HBS) in oceanic environments. The focus is on the determination of the envelope of hydrate stability under conditions typical of those related to the construction and operation of offshore platforms.

Scope of Work

To achieve the objectives of the proposed study, the following approach is being employed:

1. The geomechanical behavior of oceanic HBS is being investigated using pore-scale models (conceptual and mathematical) of fluid flow, stress analysis, and damage propagation.
2. Laboratory studies are being conducted to (i) evaluate the conceptual pore-scale models, (ii) calibrate the mathematical models, (iii) determine dominant relations and critical parameters defining the geomechanical behavior of HBS, and (iv) establish relationships between the geomechanical status of HBS and the corresponding geophysical signature.
3. A robust numerical simulator of hydrate behavior in geologic media has been coupled with a commercial geomechanical code, thus developing a numerical code for the stability analysis of HBS under mechanical and thermal stresses.
4. Numerical studies are being conducted to analyze the HBS stability performance under conditions (i) representative of an offshore platform installation and operation, and (ii) typical of oceanic hydrate accumulations under production.

Organizations

There are four organizations initially involved with this project. These four are as follows:

- Texas A&M University (TAMU)
- University of California at Berkeley (UCB)
- Lawrence Berkeley National Laboratory (LBNL)
- Schlumberger (SLB)

4. Project Milestones

Status of Milestones for Phase II as of October 31, 2007

- The conceptual model developed within Phase One of the project has been verified against published laboratory test data.
- The quasi-static grain-scale model of HBS has been extended to incorporate tangential contact forces at grain-to-grain contacts.
- The performance of the computations has been significantly enhanced by development and implementation of customized algorithms.
- We submitted a topical report entitled "Approach to Forming Hydrate Bearing Samples in Fine-Grained Material".
- The approach recommended for building samples and testing those samples was approved by the DOE.
- We designed and completed fabrication of a geomechanical properties and geophysical signature test cell.
- We tested the seismic transducers to be used in the test cell.
- We attended and made several presentations at the DOE Program Review.
- We used TOUGH+Hydrate to simulate gas production from the Messoyakha gas field in Russia.
- We performed gas production parametric studies that will be valuable when using TOUGH+Hydrate-FLAC3D to explore seafloor stability issues.
- The interface between PETREL and FLAC3D has been developed.
- The workflow to extract data from PETREL and use it in FLAC3D has been designed.

5. Results of Work During the Reporting Period

<u>Task 6 – Fundamental studies of pore-scale geomechanical behavior Part II</u>

Phase I work highlighted the importance of the tangential contact forces for adequate simulation of deformation of granular media. Significant part of the effort was focused on extending the model by incorporating tangential contact forces from Mindlin's theory (Mindlin, 1949, Mindlin and Deresiewicz, 1953). As a result, the estimates of Poisson's ratio and shear elastic moduli became close to the numbers reported in the literature.

To gain capability to handle both elastic phenomena and rock failure of micro-mechanical simulations, the normal and tangential contact forces have been complemented by introduction of slip. The possibility of slip is characterized by Mohr-Coulomb criterion. Implementation of this model in simulations has been started. New customized algorithms made possible to run very complex simulations on a personal computer.

The impact of hydrate dissociation on rock strength has been modeled by simulation of reduced effective stress and weakening of the solid skeleton by "melting" hydrate clusters. Simulations show noticeable reduction in shear modulus. The developed model is based on quasi-static approach. We have found that it produces more stable grain packs than simulations based on DEM approach.

The strain in a granular medium is the result of deformations and rearrangements of the grains. The stress sums up from numerous contact forces between the grains. The magnitudes and orientations of these forces are highly variable from contact to contact. The nature of these forces also is variable. Each grain-to-grain interaction includes contact deformations of the grains in contact, friction, and cement-bond stress. Hertzian contact theory adequately describes normal component of small elastic deformation at the contact between two spherical grains. Mindlin's extension of this theory (Mindlin, 1949; Mindlin and Deresiewicz, 1953) provides a model for small contact deformations accounting for tangential forces and friction as well. Bond stiffness can be modeled by assigning different elastic moduli to a small amount of cementing material near the inter-granular contact. The previous semi-annual report includes development of a model including normal contact forces. In this report, this model is extended to incorporate tangential forces and slip. The next step will be incorporation of cement bonds.

The importance of slip in grain-scale simulations of HBS deformation and damage is determined by several reasons. As long as the grains are stuck at the contacts, the formation behaves as solid rock. However, as the distribution of the contact forces changes due to hydrate dissociation, the number of contacts where slip occurs grows up dramatically. Such inelastic transformation at macroscopic scale may mean, in terms of macro-scale, rock fracturing, failure, or even liquefaction. All these transformations dramatically alter the strength of the formation. Initially solid rock transforms into mechanically weak material prone to failure, and unwanted catastrophic consequences for the off-shore infrastructure may result.

An ultimate answer to the question about stability of the slope of the ocean bottom can be provided only by large-scale simulations coupling fluid flow and rock mechanics. However, such simulations require input in the form of trend curves, which are ultimately determined by the micromechanics of the medium. The results in this report provide fundamental machinery for simulation of HBS deformation with slip. We model the mechanical deformation of HBS or, more generally, of a granular medium, by numerical simulations of a pack of elastic spherical grains. Although this approach cannot entirely displace laboratory tests as the ground truth, it offers some opportunities which may be not available otherwise. Grain-scale simulations provide unique insights into the processes and phenomena underlying the classical continuum-medium models. Such simulations provide explanations for such known phenomena as strain hardening and irreversibility. Moreover, they can be used to play various what-if scenarios, which cannot be performed in a laboratory.

The classical theory of elasticity is a conventional tool to characterize the strength of the rock. However, in the context of the current project, this approach is insufficient. The dissociation of hydrate clusters, accumulation of breaking inter-granular bonds, dramatically alters the mechanical properties of the rock. Liquefaction can transform solid rock into unstable sand. Grain-scale simulations can handle simultaneously the elastic deformations of the formation, and damage propagation and failure of the rock (Jin et al., 2003, 2004; Jin, 2006). Our quasi-static approach, where deformations are modeled as series of mechanical equilibrium configurations, leads to robust and efficient computational algorithms.

The results have been presented at three conferences and three invited seminars.

- 03/22/2007 Mechanics of Natural Rocks at a Microscopic Scale. University of Stavanger, Norway – Dmitriy Silin
- 04/2/2007 Poster at the 2007 AAPG Annual Convention in Long Beach, CA – Ran Holtzman
- 04/4/2007 talk at SPE 2007 Western Region Student Paper Contest, Long Beach, CA – Ran Holtzman
- 06/14/2007 Seminar at the Department of Environmental Sciences and Energy Research, Faculty of Chemistry, Weizmann Institute of Science, Israel – Ran Holtzman.
- 06/19/2007 Seminar at the Department of Geological & Environmental Sciences, Ben Gurion University of the Negev, Beer Sheva, 84105, Israel – Ran Holtzman
- 06/29/2007 Seminar at the Geophysics Department, Earth Sciences Division, Lawrence Berkeley National Laboratory, Berkeley CA – Ran Holtzman
- 07/24/2007 talk at the USA Computational Mechanics (USACM) conference in San Francisco, CA

Task 7 – Developing Data Sets for Hydrate Deposits in Deep Water

Starting with a PETREL dataset, the objective of this work is to provide software tools and describe a workflow for the creation of a FLAC3D model ready-to-run. The PETREL model contains, among other things, the description of horizons and the special distribution of properties. As part of this project, an automatic method of creating a FLAC3D grid must be developed. The resulting grid must be composed of multiple materials representing the various regions of the PETREL database delimited by the horizons.

In addition to the grid, an automatic and conservative method of extracting material properties from PETREL should also be devised. The extracted properties should be automatically assigned to the individual FLAC3D grid element. The user will complement the missing material properties and mechanical behavior law parameters by adding them manually to the FLAC3D data file.

A number of comments are in order.

- Data sets extracted from PETREL may be very large. An automatic method should be devised to coarsen (decimate) the data, while maintaining pertinent details.
- The PETREL model may contain features ranging in size from tens of meters to hundreds of kilometers. This requires a non-traditional meshing approach that would keep the total element count in the FLAC3D model to a minimum while ensuring adequate representation of details and adequate transition between FLAC3D element sizes.
- Property transfer from PETREL to FLAC3D should be conservative
- The workflow should be simple and robust

FLAC3D and the 3DShop option

FLAC3D is a numerical modeling software for the advanced geotechnical analysis of soil, rock, and structural support in three dimensions. FLAC3D is used in analysis, testing, and design by geotechnical, civil, and mining engineers. It is designed to accommodate any kind of geotechnical engineering project where continuum analysis is necessary. FLAC3D uses an explicit finite volume formulation that models complex behaviors not readily suited to finite element software, such as problems consisting of several stages, large displacements and strains, non-linear material behavior and unstable systems (yield/failure over large areas, or total collapse, etc.).

FLAC3D version 3.1, combines speed (using multithreading on multiple processors, see multiprocessor speedup in (Figure 2), virtually unlimited model size (with the new 64 bit implementation), and geometrical flexibility (with its ability to create both hexahedral and tetrahedral grids using the 3DShop option).

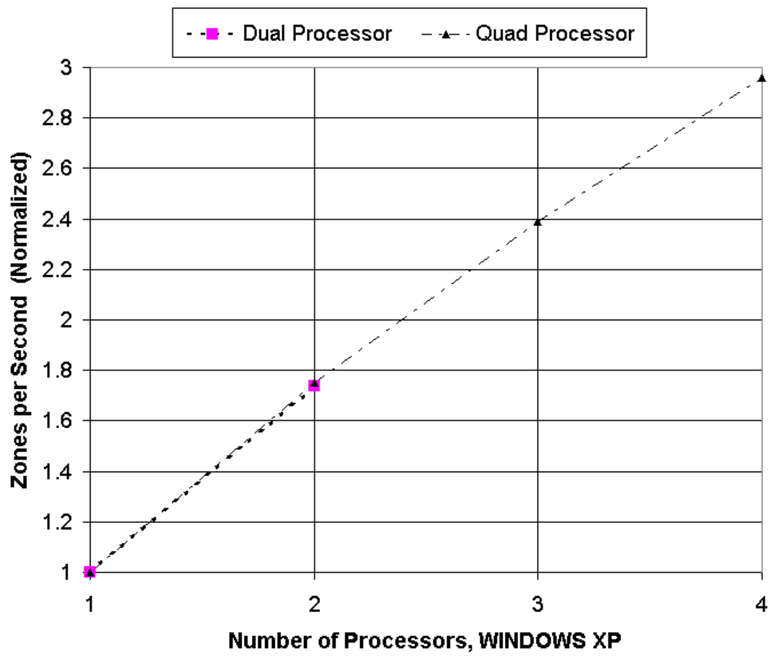

Figure 2 – FLAC3D 3.1 Parallel performance: multiprocessor speedup as a function of number of processors

In addition to hexahedral grids, FALC3D 3.1 accepts more complex models using tetrahedral grids supported with the Nodal Mixed Discretization (NMD) scheme which ensures accurate plasticity results for tetrahedral grids. 3DShop's local mesh refinement facility allows for a more economical use of memory by concentrating elements near areas of interest.

The 3DShop option of FLAC3D is a powerful solid modeler that can be used to import complex models or create them from scratch. 3DShop includes an automatic hexahedral and tetrahedral grid generator for FLAC3D (Figure 3).

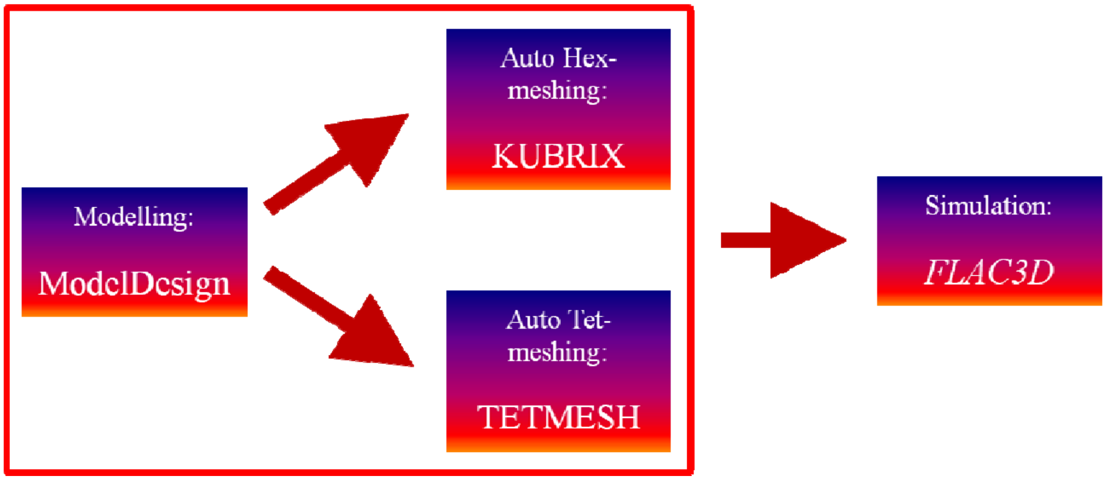

Figure 3 – Organization of 3Dshop

In contrast to many solid modelers used in mechanical engineering, 3DShop can handle complex non-manifold surfaces commonplace in geotechnical engineering applications. CAD and GIS data can be read from a variety of geotechnical analysis and mechanical computer-aided engineering tools such as GoCad, Vulcan, Map3D, DataMine, AutoCad, SolidWorks, SolidEdge, ProEngineer and Catia through the STEP, IGES, 3DS (3DStudio), STL, VRML, DXF and DWG (AutoCad) file format to produce both hexahedral and tetrahedral grids (Figure 4).

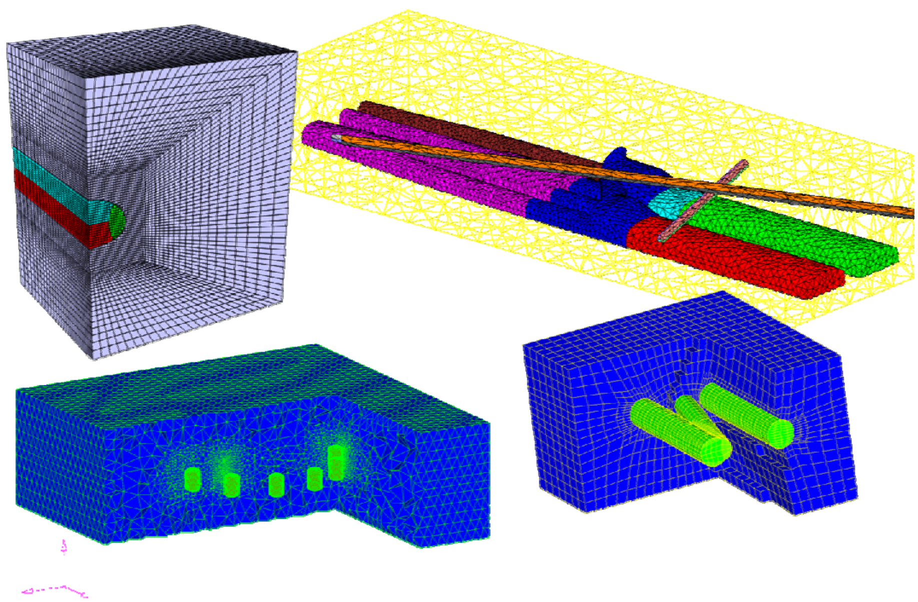

Figure 4 – Geometrical flexibility in FLAC3D 3.1 with hexahedral and tetrahedral grids

Importing Horizons into 3DShop

As part of the present project, a module was developed to read and parse zmap files. This functionality enables users to export horizons from PETREL as zmap files and read them into 3DShop. In future developments the more straightforward import of horizons as .grid files may be envisaged.

Imported horizons can be visualized in 3DShop and saved as a single STL file. An STL file is an ASCII file used to store triangular element information. If the horizons cover a wide area and as a result their triangle count is large, 3DShop allows for the automatic coarsening or decimation of these meshes.

Data decimation

The decimation procedure substantially reduces the number of triangles in an imported horizon file while maintaining small details. The decimation process starts with the selection of a threshold dihedral angle by the user (usually in the order of 5°) and proceeds as follows:

- Sorting of all edges where the edge is the smaller of the two other edges in each of the adjacent triangles
- Sorting of the previous list in the order of increasing dihedral angles
- Collapse of all edges and their corresponding adjacent triangles, up to the threshold dihedral angles specified by the user
- This procedure is iterated several times until no edge collapse is possible

An example of the outcome of this procedure for a given horizon is shown in Figure 5. It can be noted that this decimation approach preserves details while reducing the triangle count by nearly an order of magnitude.

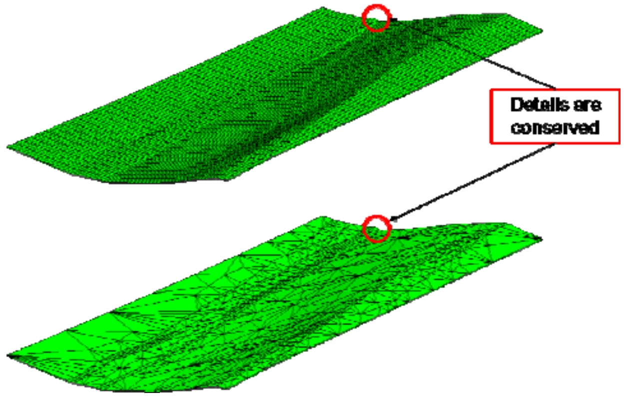

Figure 5 – zmap file translation and subsequent mesh decimation

After reading all the horizons, the assembled geometry can be visualized in 3DShop (Figure 6).

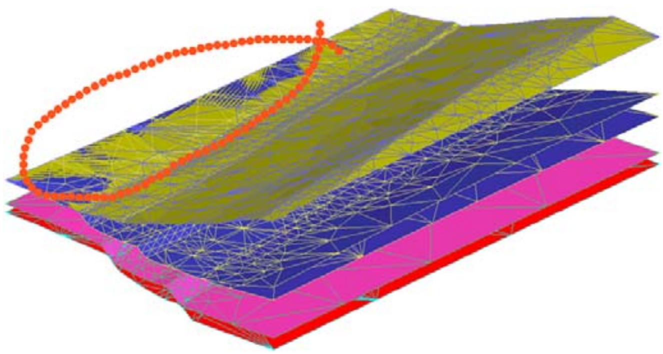

Figure 6 – Final assembled horizons. Highlighted are show two or more tangent horizons.

A closer look at Figure 6 shows that the geometry of the assembled horizon presents a major challenge. The highlighted area shows that two or more horizons are tangent. This represents a challenge for traditional solid modeling where surfaces should intersect at clear edges without causing topological ambiguity or any angle close to zero. If we were to clean up this geometry, we would have to decide where the intersection of the horizons occurs, and assume a clean description of the intersection curve. This would require manual intervention. The Oct-tree meshing approach avoids this problem.

Oct-tree Mesh Generation

Mesh generation should not require any operator intervention. This leaves us with any of the available automatic meshing options. But automatic meshing requires the creation of a so-called solid model. This requirement can also be described as that of creating a watertight triangulation of all the surfaces constituting the horizons and the outer block. Because of the topological ambiguity due to tangent horizons, we propose an oct-tree mesh generation technique.

Oct-tree meshing follows these steps:

1. Determination of a bounding cube. This cube is called the root element
2. If this element intersects the horizon, subdivide it into 8 cubes
3. If the edge length of the cube is smaller than a user-specified value, STOP
4. Else, go to step 2.

Because of its simple structure, the oct-tree mesh has a simple data structure depicted in Figure 7.

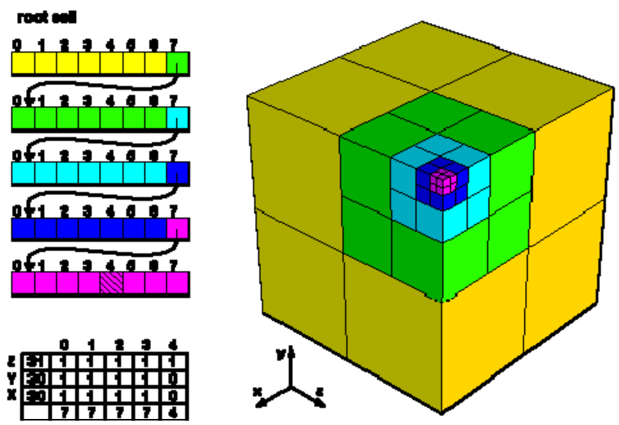

Figure 7 – Data structure of an Oct-tree mesh

With an Oct-tree mesh, the size of the smallest captured detail is about the size of the smallest cube of the oct-tree; in the example above, the size of the pink cube.

The Oct-tree is first used to detect the geometry. Figure Figure 8 shows a 2-D illustration of this approach. The blue region is the oct-tree's interpretation of the geometry.

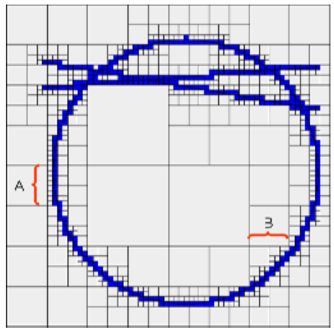

Figure 8 – Principle of Oct-tree geometry detection

The standard oct-tree can cause abrupt grid refinements. The A region of Figure 8 shows an abrupt 1 to 8 refinement and region B show an asymmetrical 1 to 3 refinement. These types of mesh refinement, while supported in FLAC3D, introduce large errors and are not recommended A balanced Oct-tree is one in which all refinements are 1 to 2 in 2D and 1 to 8 in 3D (Figure 9). These types of refinement are preferable.

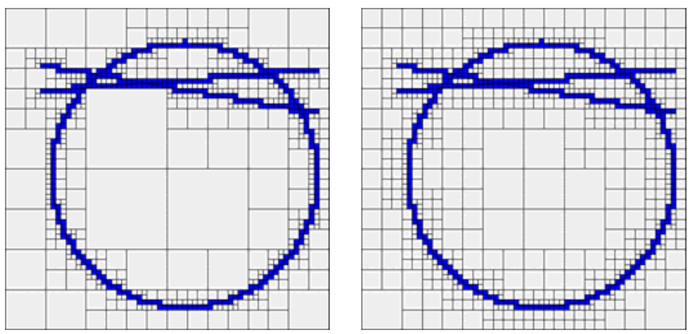

Figure 9 – Original (unbalanced) and balanced Oct-tree. In a balanced oct-tree, two adjacent cubes are always no more than one generation apart.

The dark blue region delineates the various regions. The next step is to identify the regions as shown in Figure10.

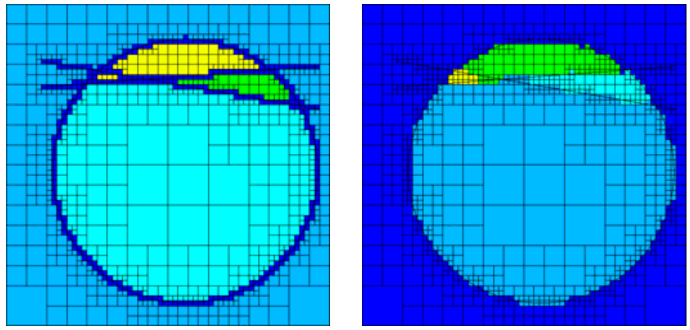

Figure 10 – Partition of the space using an oct-tree. Left: regions + boundary. Right: regions

The oct-tree approach is very economical in terms of element count. Figure 11 shows the increase in number of elements as cubes are cut into smaller and smaller pieces. In the limit, the number of elements is multiplied by 4 every time cube splitting advances one generation.

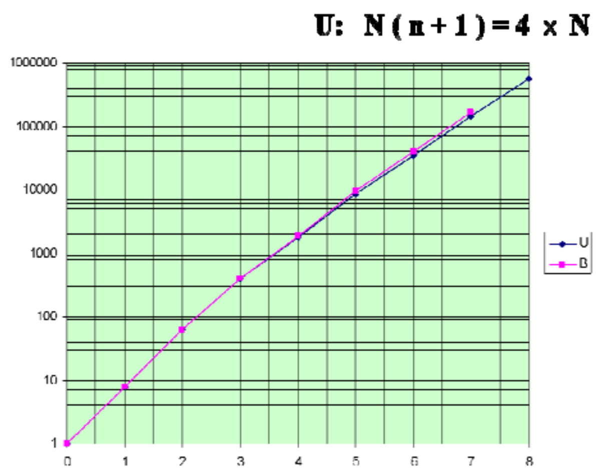

Figure 11 – Number of elements as a function of oct-tree generations. U represents an unbalanced oct-tree while B is a balanced one which results in a larger number of elements

In the present test case, the model's geometrical features vary in size from 30 to 3000 m. As a result, the number of oct-tree generations will be in the order of:

$$\mathbf{N = \log (3000/30) / \log 2 = 6}$$

FLAC3D is one of the only commercial software packages that can handle oct-tree meshes because it can handle so –called dangling nodes. FLAC3D requires some overhead to handle such grids but all in all, using oct-tree grids results in substantial savings in memory and CPU time requirements. Figure 12 shows the present model meshed with a 7 level Oct-tree mesh. Figure 13 shows a complex salt dome structure meshed with the same technique.

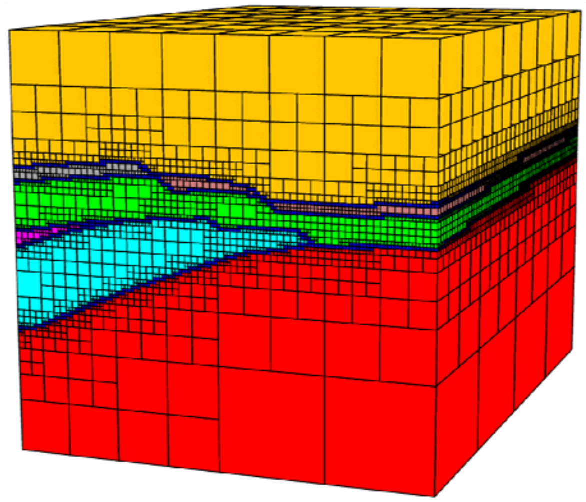

Figure 12 – The present model meshed by a 7 level oct-tree

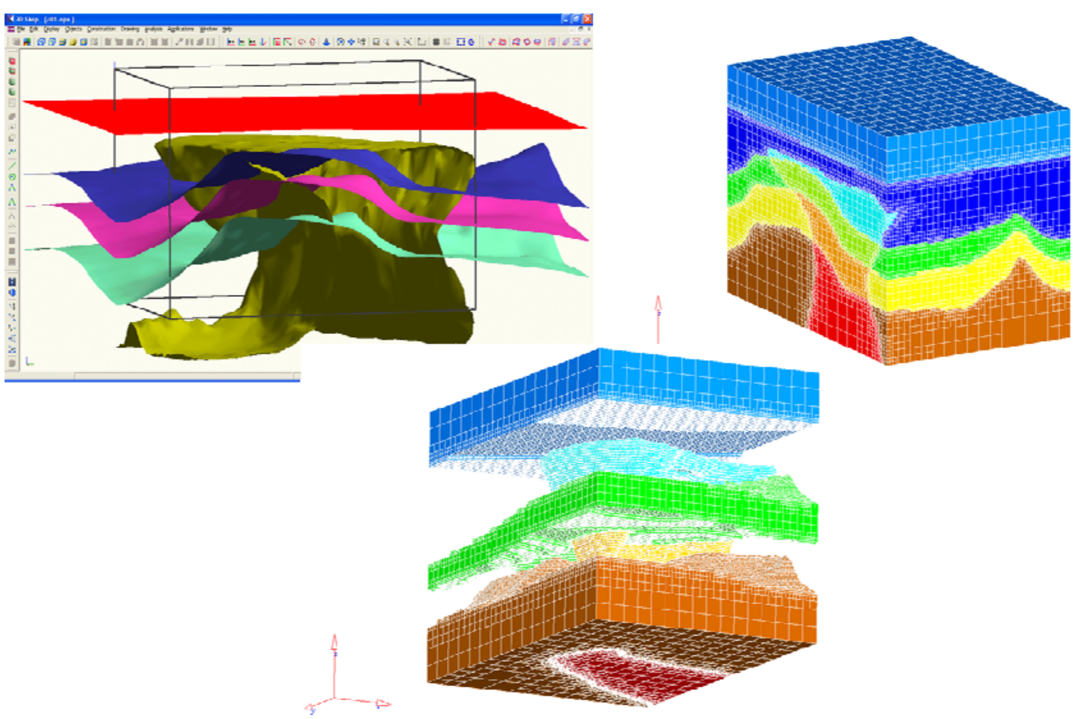

Figure 13 – Example of a salt dome meshed with oct-trees

To verify that the oct-tree mesh results do not introduce any spurious artifacts in the results, we modeled the complete geometry as a single homogeneous elastic material, and computed the stresses caused under its own weight. A vertical cross-section trough the middle of the geometry is shown in Figure 14. It can be seen that artifacts caused by the oct-tree mesh do not exceed the local maximum element size.

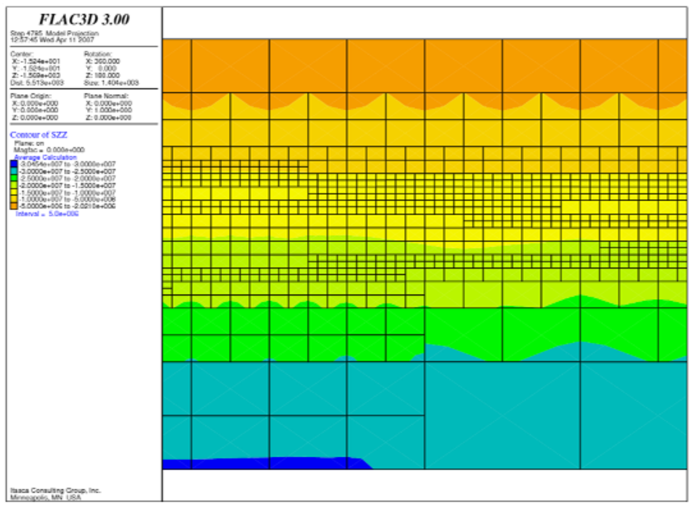

Figure 14 – Contour of vertical stress SZZ for the present model represented as homogeneous elastic material.

PETREL grid extraction

In practice, material properties are extracted from a .grid file outputted by the PETREL database. The following guidelines should be creating when creating a .grid file:

1. Make sure that the grid file contains only the properties that you intend to read
2. The dimensions and location of the parallelepiped containing the model (for which the .grid file is produced) should match those of the parallelepiped containing the horizons
3. Grid orientation must be direct with the Z-direction pointing upwards

The grid file is read by 3DShop during mesh generation. If a material is available in the grid file, it will be read by 3DShop.

PETREL property extraction

A key concern in extracting material properties is that the property assignment be conservative. To comply with this requirement, we have implemented a method in 3DShop that computes, for each FLAC3D element, its volume intersection with all the PETREL cells concerned. For each PETREL cell P_i intersecting the FLAC3D element φ, its contribution to the FLAC3D element φ is weighed by the volume of intersection. The sum of all contributions is the FLAC3D element property (Figure 15).

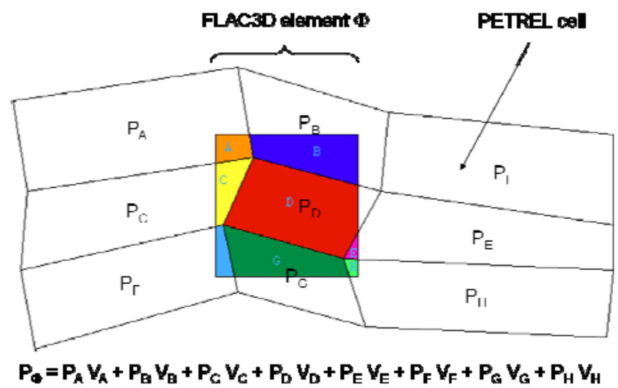

Figure 15 – Computation of the FLAC3D element property based on PETREL cell properties

As properties are calculated for each FLAC3D element, 3DShop adds the property of that element to an ASCII file. Once mesh generation is complete and FLAC3D is launched, FLAC3D uses a FISH function to read the property file and assign the right property to each element.

Sample Calculation

An elastic model is used and several typical material properties are assigned to the various layers between the horizons. The FLAC3D data file is shown below.

```
;Schlumberger ECLIPSE-FLAC3D Data Transfer test case created by Reza Taghavi 3/27/07


res a1_lev7.sav

model elastic

group sandstone1 range group group4
group sandstone2 range group group5
group sandstone3 range group group3
group mudstone1  range group group9
group mudstone2  range group group6

;All groups other than sandstone 1, 2 & 3 and mudstone 1 & 2 are joints
prop bulk 4.17E+08 shear 4.55E+08 density 2710
;coh 0 fric 3.00E+01 tension 0

prop bulk 8.03E+09 shear 6.53E+09 density 2310 range group sandstone1
;coh 1.50E+07 fric 4.10E+01 tension 1.50E+06 range group sandstone1

;group 5 sandstone 2
prop bulk 1.33E+10 shear 1.00E+10 density 2310 range group sandstone2
;coh 2.00E+07 fric 4.90E+01 tension 2.00E+06 range group sandstone2

;group 6 sandstone 3
prop bulk 1.17E+10 shear 8.42E+09 density 2420 range group sandstone3
;coh 2.30E+07 fric 4.30E+01 tension 2.30E+06 range group sandstone3

;group 14 mudstone 1
prop bulk 3.22E+10 shear 6.48E+08 density 2710 range group mudstone1
```

```
;coh 1.20E+07 fric 4.70E+01 tension 1.20E+06 range group mudstone1

;group 17 mudstone 2
prop bulk 6.62E+09 shear 6.98E+09 density 2710 range group mudstone2
;coh 1.90E+07 fric 3.00E+01 tension 1.90E+06 range group mudstone2

set gravity 0 0 -9.81

;Apply Uniform Boundary Stress Field Values
fix x range x -2 2
fix x range x  1767  1771
fix y range y -2 2
fix y range y  1248 1252
fix x y z  range z -2203 -2197

;1000 kg/m3 * 1333 meters * 9.81 = 13.07e6 = pressure
apply nstress -13.07e6 range x 2 1767 y 2 1248 z -1500 -900
hist unbal
plot show base

save a1_lev7_Elastic_preSolve.sav
solve
save a1_lev7_Final.sav
ret

define TranslateAndScaleToMeters
   gp = gp_head
   loop while gp#null
      gp_xpos(gp) = 0.3048 * ( gp_xpos(gp) - 1643300 )
      gp_ypos(gp) = 0.3048 * ( gp_ypos(gp) - 9730950 )
      gp_zpos(gp) = 0.3048 *   gp_zpos(gp)
```

```
      gp = gp_next(gp)
   end_loop
end

impgrid a1_lev7.flac3d
TranslateAndScaleToMeters
del range group group2
attach face tol 1.
save a1_lev7.sav
```

Figure 16 shows the generic group assignments as produced by 3DShop. The arrowed numbers in Figure 17 refer to the new group definitions in the FLAC3D data file. Figure 18 Shows the FLAC3D grid after removal of the group corresponding to the material “water”. This is done in the FLAC3D data file. Please note that it this test case, properties are not read from PETREL but assigned explicitly in the FLAC3D data file.

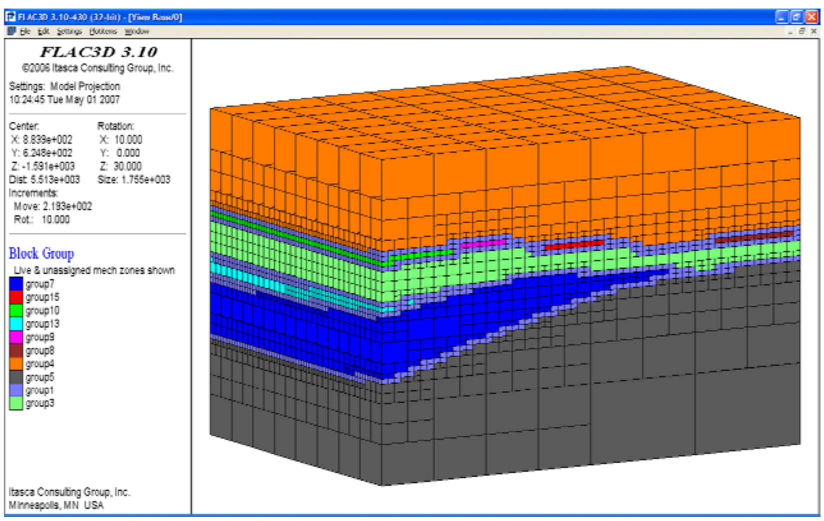

Figure 16 – Sample calculation grid

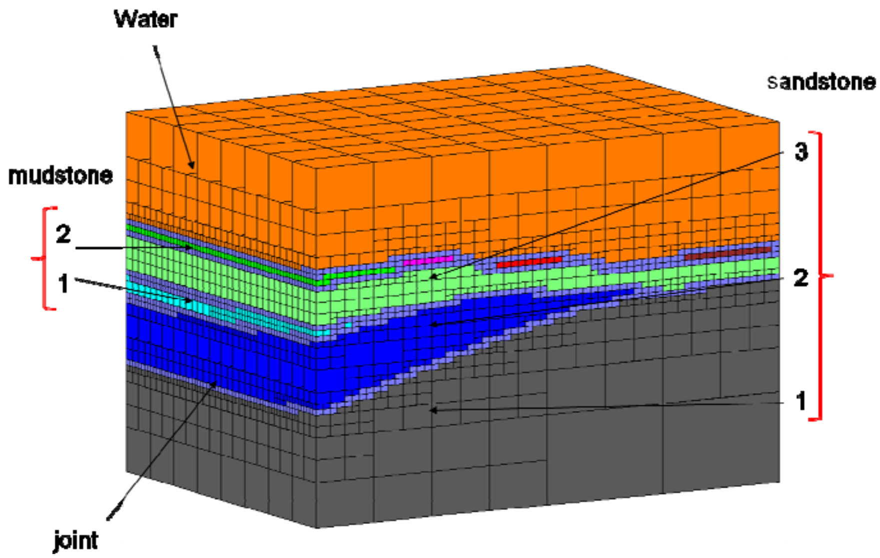

Figure 17 – New group assignments done in the FLAC3D data file

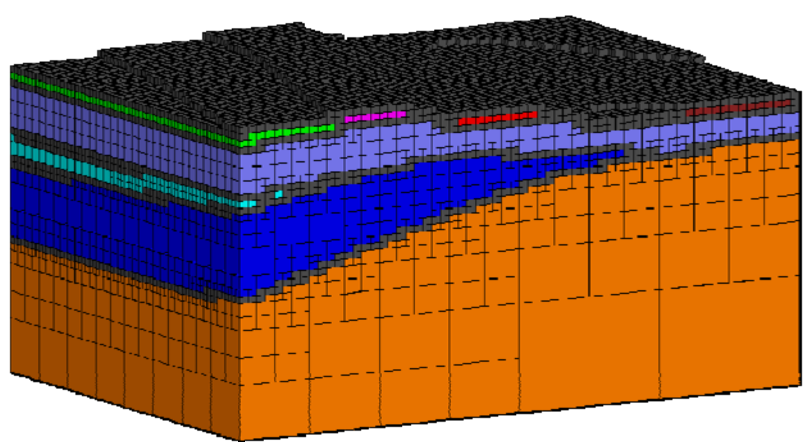

Figure 18 – The final FLAC3D grid after removal of "water"

Figure 19 shows a result of this simulation

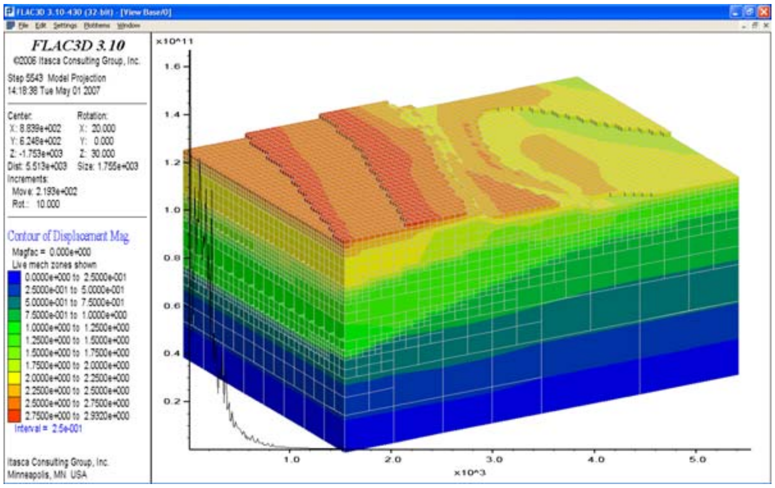

Figure 19 – Sample elastic calculation: contour of displacement magnitude

PETREL to FLAC3D Workflow

Figure 20 shows a flow chart of the workflow. Yellow rectangles represent the development work performed in the framework of the present project. Light-blue squares are files and orange squares represent existing software applications.

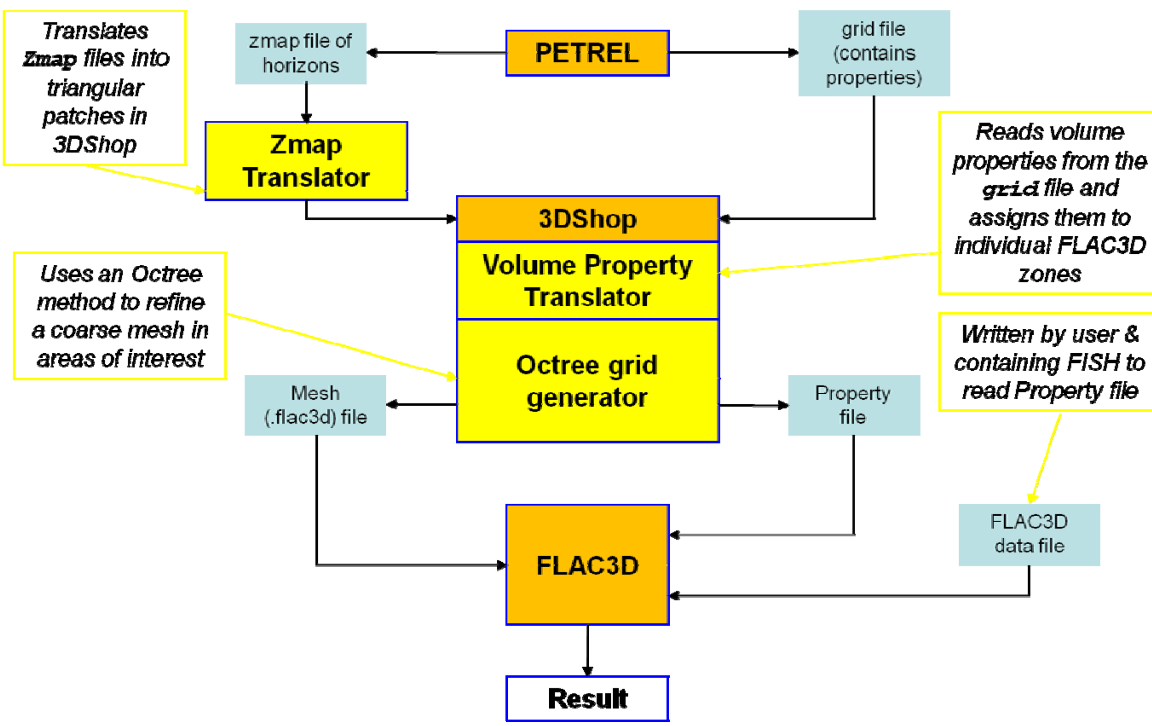

Figure 20 – PETREL to FLAC3D Workflow Diagram

The various steps involved in creating a working FLAC3D model are as follows:

I. Collecting Geometry and Translation into STL files

1. Collect the following items
    1. **Grid file**. In PETREL, export a grid file representing a parallelepiped. The file must contain the properties that you are would like to assign to FLAC3D elements (porosity, density, etc…). All dimensions are in feet.
    2. **Horizons in the zmap format.** The file must cover the same parallelepiped, with all dimensions in feet.

II. Translate the horizons:

1. Run**:**

    Kubrix –i waterbottom –it zmap –translate stl

    This produces a file called **x.stl**
2. Rename **x.stl** to **w.stl (mv x.stl p1.stl)**
3. Run:

    Kubrix –i pleist1 –it zmap –translate stl
4. mv **x.stl p1.stl**
5. repeat the same operation with pleist2, unconform1 and unconform2
6. …….

At the end, we have 5 files: **w.stl, p1.stl, p2.stl, u1.stl, u2.stl**

III. Creating the Horizon Model & Determining the Extent of the FLAC3D Grid

1. Run 3DShop
    1. Create a new document
    2. Insert **w.stl, p1.stl, p2.stl, u1.stl, u2.stl** in the new document
    3. Save the complete model as: **a1.stl**
    4. Reflect the entire model with respect to the z = 0 plane
    5. Save the complete model, again, as: **a1.stl**

    You have created the input geometry
2. Determine the box containing the FLAC3D mesh…

1. Determine the smallest and largest x,y and z of the model using 3DShop.

IV. Create the FLAC3D Mesh Based on a1.stl (Preparation)

3. Run 3DShop…
    1. Read in **a1.stl**
    2. Select **Applications|kubrix|Hexahedral Meshing.** The Hexahedral Meshing dialog box opens…
    3. Click on Default to enter default values in all fields
    4. Enter the following string in the field marked New Keywords:

-mode octree -olevel 5 -obox 1646200 9733000 -5220 5800 4100 4000 -app petrel

5. **Mode:** specifies the custom Octree mesh type
6. **Olevel:** specifies the level of Octree mesh generation
7. **Obox**: specifies the position of the box: the first 3 floats are the coordinates of the center of the box and the next 3 indicate the dimensions of the box
8. **app:** specifies the custom application

V. Create the FLAC3D Mesh Based on a1.stl (Mesh Generation)

4. Click on Compute…
    1. 3DShop reads **a1.stl**
    2. Creates and octree mesh that fits in the box specified by **obox** with **olevel** number of levels
    3. Parses the grid file, extracts the cells
    4. Extracts the properties
    5. Computes the contribution of each PETREL cell to each FLAC3D element
    6. Outputs PetrelProperties.dat
    7. Outputs a1.flac3d

VI. Output from 3DShop

```
PORO
0.086446
0.0812567
0.0964004
.
.
.
.
0.0813897
0.0840277
0.0865843
0.0791058
DENSITY
1.13922
1.06322
1.26
1.18523
1.21041
.
.
.
.
1.06196
1.19866
1.20858
1.07038
```

```
*
* FLAC3D input deck produced by KUBRIX version 9.3.0
* mesh built: Thu May 03 07:14:01 2007
* -app 3dshop -i C:\Documents and Settings\Reza Tagh
Taghavi\Desktop\Itasca\geo\Schlumberger032307\a1.fla
-obox 1646200 9733000 -5220 5800 4100 4000
*
*GRIDPOINTS
G 1, 1.643300e+006, 9.730950e+006, -7.220000e+003
G 2, 1.649100e+006, 9.730950e+006, -7.220000e+003
G 3, 1.649100e+006, 9.735050e+006, -7.220000e+003
G 4, 1.643300e+006, 9.735050e+006, -7.220000e+003
.
.
.
.
G 11593, 1.648919e+006, 9.734922e+006, -4.470000e+00
G 11594, 1.649100e+006, 9.734922e+006, -4.470000e+00
G 11595, 1.648919e+006, 9.735050e+006, -4.470000e+00
*ZONES
Z B8 1, 9, 47, 35, 36, 48, 37, 49, 50
Z B8 2, 47, 2, 48, 49, 51, 50, 52, 53
Z B8 3, 35, 48, 10, 37, 54, 41, 50, 55
.
.
.
Z B8 8889, 11577, 11578, 11589, 11581, 11590, 11593,
Z B8 8890, 11583, 11589, 11585, 11587, 11591, 2324,
Z B8 8891, 11589, 11590, 11591, 11593, 11592, 11595,
*GROUPS
ZGROUP group1
1290 1292 1293 1294 1295 1300 1302 1304 1305 1306 13
1318 1319 1320 1321 1323 1328 1330 1336 1337 1338 13
.
```

Figure 21 – PetrelProperties.dat and a1.flac3d files

VII. Running FLAC3D

1. Run FLAC3D
2. Run ReadPetrelProperties.fis
3. Remove water
4. Attach face **tol 1**
5. Complement missing properties
6. Manage model through FISH

Task 8 – Laboratory studies of basic rock properties in oceanic hydrate bearing sediments

Completion of Design and Fabrication of Geomechanical Properties and Geophysical Signature Test Cell

LBNL designed and completed construction of a geomechanical test cell (Figure 22) for use in measuring the geomechanical properties and geophysical signature of hydrate-bearing sediments. The cell body is composed of aluminum to allow CT scanning, and the end caps are composed of stainless steel. The cell properties are listed in Table 1. The cell was designed primarily for use with synthetic methane hydrate samples. The engineering note for the vessel is under development prior to pressure testing. An exterior jacket is being constructed for temperature control.

Table 1. Geomechanical Property and Geophysical Signature Cell Properties

Sample Size	3.8 cm dia x 10.8 cm (1.5 in x 4 in)
Loading	Confining stress up to 48 MPa (7,000 psi) Axial stress up to 270 MPa (39,000 psi). Allows testing a wide range of samples by both low-axial stress and high-axial stress mode operations (double chamber design). Axial displacements are measured by an LVDT attached to the loading piston Lateral expansion is measured by confining fluid volume displacement under a constant confining stress
Seismic Measurements	Loading platens contain compressional (P) and shear (S) wave seismic transducers
X-ray CT Imaging	Low x-ray-attenuating aluminum cell wall (also serves as a load frame)

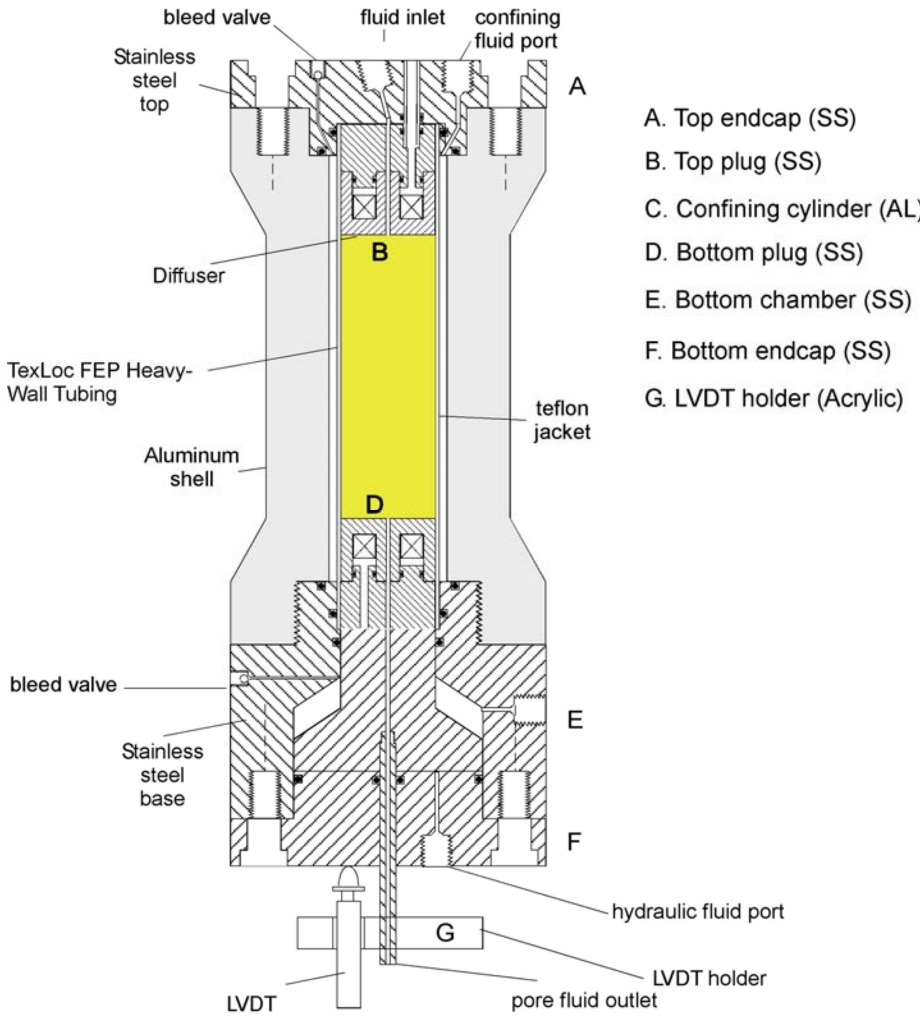

Figure 22 – Cell Schematic

Test of Acoustic System

Elements to be used in the geomechanical cell were assembled and independently tested prior to assembly in the cell. One critical component is the seismic (acoustic) source and receiver installed within the loading pistons (Figure 23). Seismic measurements will provide data regarding the mechanical property changes in test cores during hydrate formation and a loading test, which will augment and compliment x-ray CT imaging.

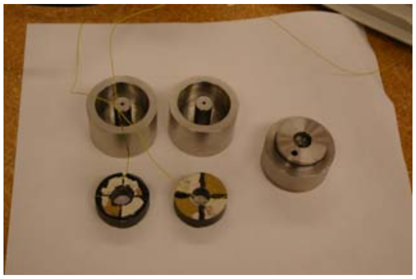

(a) Piezoelectric elements and transducer housing

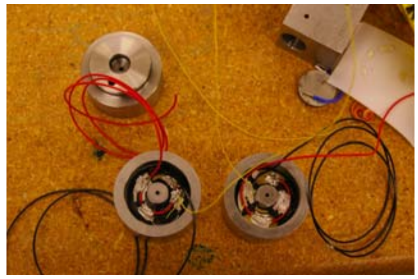

(b) Installed in the housing. Electrodes attached.

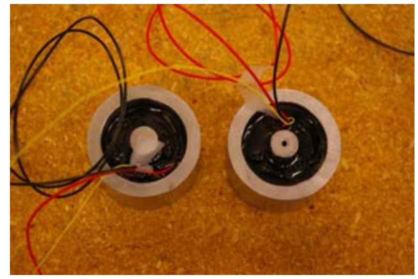

(c) Potted with epoxy for electric insulation and mechanical stability

Figure 23 – Construction of piezoceramics-based seismic (acoustic) transducers

One common problem when conducting S-wave measurements in a long core sample is the degradation of wave quality due to P-waves (travels faster than S-waves) and conversions into surface or flexural waves (causes waveform dispersion). To mitigate this problem, S-waves in our test cell uses are generated via torsion mode rather than commonly used polarized shear mode. The quality of the seismic signal was tested across an acrylic cylinder, using lead foil between the acrylic and the platens to aid in contact (Figure 24).

Figure 24 – Testing seismic signal quality using an acrylic core.

The stainless steel cylinders at the top and the bottom of the sample house piezoelectric elements and serve as transducers. These are the actual components of the new, hydrate-testing cell under construction. Using the seismic transducers, two types of source excitation methods were used. The first method drove the source element by a square-shaped high-voltage pulse. By choosing an optimal pulse width, the piezoelectric element is brought to resonance, generating large-amplitude seismic waves. This method has an advantage of generating large amplitudes. However, the waves are limited to relatively high frequencies (~200 kHz). Examples of P- and S-wave signals using the resonant-mode excitation are shown in Figure 25.

An alternative method is to drive the source quasi-statically using electric signals with arbitrary shapes. This has an advantage of generating waves with a broad band of frequencies, though the resulting signal amplitudes are generally small. For testing attenuating (high-loss) materials, the amplitude loss of high-frequency waves during propagation may be more disadvantageous than the initial small amplitude of low-frequency waves. Using this technique, we have identified the optimal excitation frequencies to be used for the measurements, based upon the quality of measured seismic pulses. For P-waves, this was 200 kHz, and for S-waves, 50 kHz. The relatively long wavelength resulting from the S-wave's lower frequency should help to reduce expected degradation of signal quality due to scattering by heterogeneities within a hydrate-bearing sediment core.

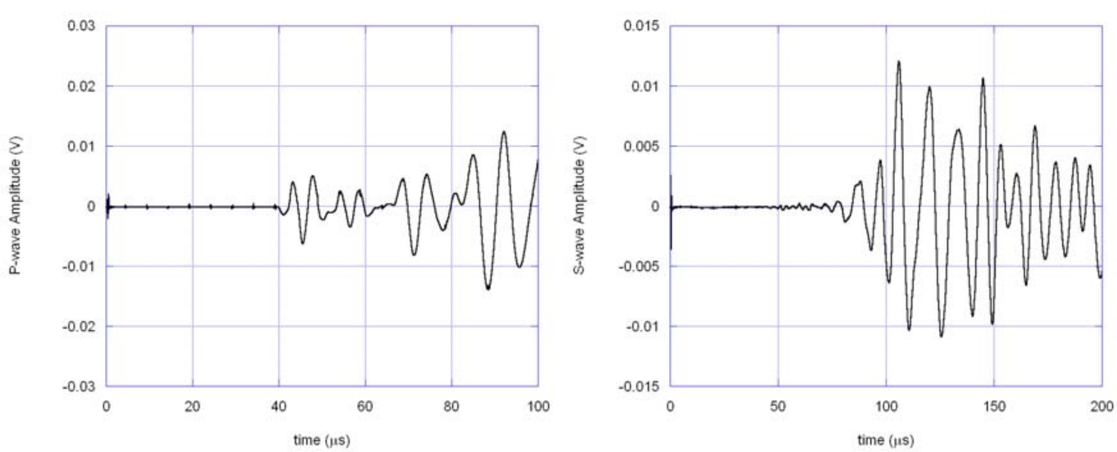

(a) P-wave signals (1^{st} arrival~40 μs) (b) S-wave signals (1^{st} arrival~77 μs)

Figure 25 – Seismic signals measured using resonant-mode excitation of the source.

Presented Projects at the Program Review

- George Moridis and Tim Kneafsey attended the DOE Methane Hydrate Program Peer Review held at the Colorado School of Mines, Golden Colorado, September 18-20, 2007.
- George Moridis presented "LBNL Studies on the Numerical Simulation of the Geomechanical Behavior of Hydrate-Bearing Sediments", and
- Tim Kneafsey presented "Laboratory Studies of Basic Rock Properties in Oceanic Hydrate-Bearing Sediments: Laboratory Studies in Support of Geomechanical Performance of Hydrate-Bearing Sediments in Offshore Environments".

Task 10 – Predictive studies of hydrate bearing sediment stability performance under conditions representative of an offshore platform installation and operation.

This study will have several stages. Initially, small subcomponents of the system shall be studied. With the knowledge gleaned from the first stages of the study, progressively larger and more integrated components shall be studied. These studies shall be conducted using the T+H/FLAC code (Task 4), and shall be conducted mainly by TAMU and UCB graduate students with significant input and strong involvement of LBNL.

Subtask 10.3 **Effect of gas production from oceanic hydrate accumulations on the HBS geomechanical stability, with particular emphasis on sloping oceanic terrains.** (Responsible party: TAMU, SLB and LBNL [funded under a separate Field Work Proposal])

The recipient shall apply the coupled model to evaluate scenarios concerning how production of natural gas from or near sediments containing gas hydrate deposits will affect the geomechanical stability of the seafloor in both the short term and the long term.

To prepare for simulating offshore gas hydrate production, we have decided to learn more about gas production from gas hydrates by simulating gas production from the Messoyakha gas field in Russia. This field is one where many experts believe substantial volumes of gas have been produced from the hydrates over many decades. We have found the exercise to be extremely useful by using the TOUGH+Hydrate to simulate real data from a real field. The insight gained from this work will be valuable to our efforts to simulate gas production from hydrates offshore so we can determine the effect of gas production on seafloor stability.

Summary

The Messoyakha Gas Field is located in Siberian permafrost. The field has been described as a reservoir containing free natural gas, overlain by a hydrate layer and underlain by an aquifer of unknown strength. The field was put on production in 1970, and has produced intermittently since then. Several important observations have been made concerning Messoyakha to include

- an increase in average reservoir pressure when the field was shut-in,
- perforation blocking due to the formation of gas hydrates in the free gas zone during production, and
- there has been no measurable or documented change in gas-water contact as the reservoir pressure was decreased.

It has been speculated that the increase in reservoir pressure was caused by the hydrate layer dissociation, rather than aquifer influx.

The objective of this work has been to use numerical model to analyze the observed production data from the Messoyakha field so we can learn more about how to model gas production from gas hydrates using real field data. In this study, a range of single-well 2D cross-sectional models that are representative of Messoyakha have been developed using the **TOUGH+Hydrate** reservoir simulator. The simulation results were then analyzed and compared with various field observations. Further, we have performed a parametric study of reservoir properties for a hydrate capped gas reservoir.

We were able to generate results that are very similar to the reported flow rates and pressure behavior in the Messoyakha Field. The value of absolute permeability in the hydrate layer and the lower free gas layer substantially affects the continued dissociation of hydrates during shutdown. We also modeled the formation of secondary hydrates near the wellbore that can cause a reduction in the gas flow rates. The important parameters affecting the gas production are the

formation permeability in the gas layer, the effective gas vertical permeability in the hydrate layer, the location of the perforations, and the gas hydrate saturation.

Introduction

Makogon (1981) first suggested three basic phenomena to dissociate the hydrates i.e. depressurization, thermal stimulation and inhibitor injection. These three mechanisms are demonstrated in the Figure 26.

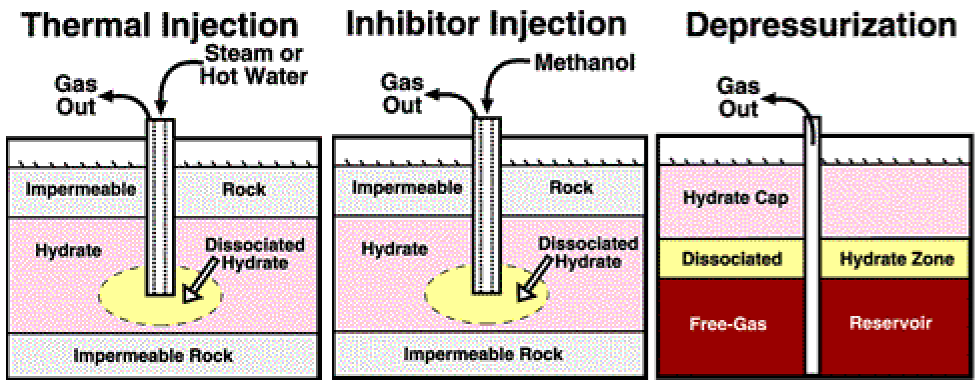

Figure 26 – Schematic of hydrate dissociation mechanisms (Courtesy: Schlumberger Ltd.)

Naturally occurring gas hydrates are divided into three main classes (Moridis and Collett, 2003, 2004). Figure 27 shows schematically the three different classes. Hydrate deposits in nature are commonly present in one of these three scenarios.

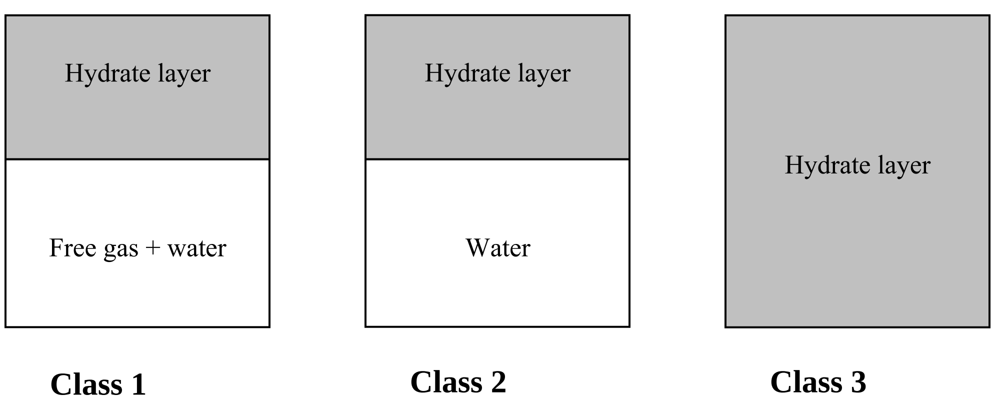

Figure 27 – Classification of hydrate deposits ((Moridis and Collettt, 2003)

In the permafrost settings, hydrates have been found in McKenzie Delta in Canada, Alaska North Slope and Messoyakha in Siberia. However, only Messoyakha Gas Field has been suggested by some experts to be producing from a hydrate capped gas reservoir. There were many observed phenomena at Messoyakha Field, which has been suggested to have occurred due to the presence of gas hydrates. The most characteristic observations were 1) the increase in the average reservoir pressure when the field was shut-in, and 2) no documented change in gas-water contact during last 30 years of production. The wells completed in hydrate layer flowed at very low rates as compared to the wells completed in the free gas zone. During the injection of methanol in certain wells, it was possible to operate certain wells at higher wellhead pressures.

The main objective of this study has been to model the various phenomena and pressure behavior at Messoyakha gas field. This will be the first study that we know of where anyone has used a reservoir simulator for studying Messoyakha Field. We started our analysis with a detailed reservoir engineering analysis of Messoyakha Field. The main of purpose of this is to reconcile the available data on Messoyakha with conceptual and fundamental knowledge of hydrates. The reconciliation study essentially was important to delineate the uncertainties in the available data. These uncertainties prompted us to develop a range of 2D cross sectional models representative of Messoyakha Field. We then simulated the gas production from these range of models to match the various observed data and phenomena. Eventually, we did the parametric study for a hydrate capped gas reservoir. We have enlisted the various controlling parameters for production from hydrate capped gas reservoirs.

Description of the Messoyakha Gas Field

The Mssoyakha gas field is under a unique thermodynamic regime in reference to natural gas hydrates. Figure 28 shows the equilibrium curve for methane hydrate and the location of the top and bottom of the Messoyakha gas reservoir. It can be seen from Figure 28 that upper part of Messoyakha reservoir is under hydrate stable region and lower part is outside the stable boundary.

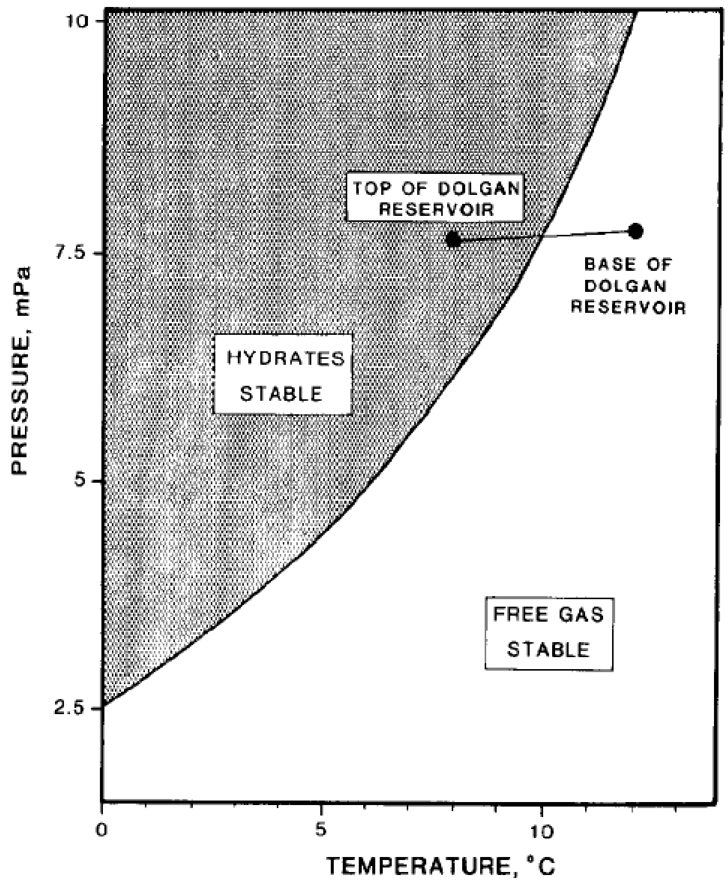

Figure 28 – Initial thermodynamic state of Messoyakha reservoir (Krason and Finley, 1992)

Geology

Messoyakha gas field is located in eastern Siberia and was discovered in 1967 (Makogon et al., 2005). A cross sectional schematic of Messoyakha is shown in Figure 29 (Makogon et al., 2005). Messoyakha gas field is enclosed in an anticlinal structural trap. The field has a 420-480 m thick permafrost zone. The producing intervals are located in Dolgan formation (sandstone) which is sealed by shale above. The Dolgan formation is interbedded with shale streaks frequently. A detailed description on Messoyakha Field can be found in several sources (Krason and Ciesnik, 1985; Krason and Finley, 1992; Makogon, 1981, 1997).

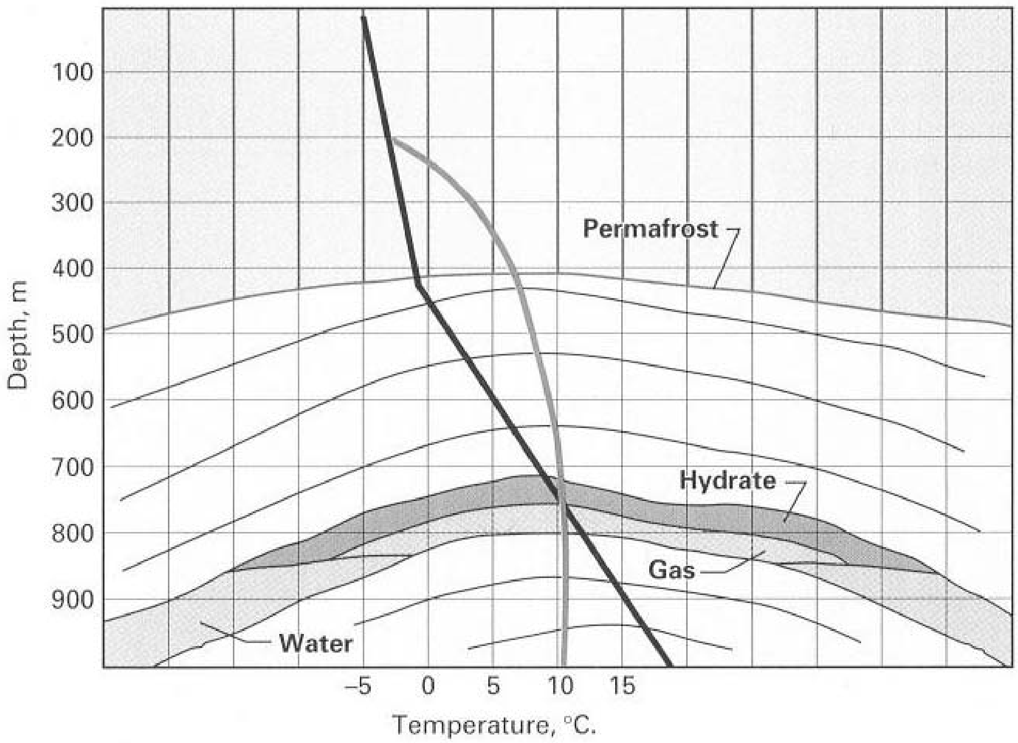

Figure 29 – Cross section of Messoyakha reservoir (Makogon et al., 2005)

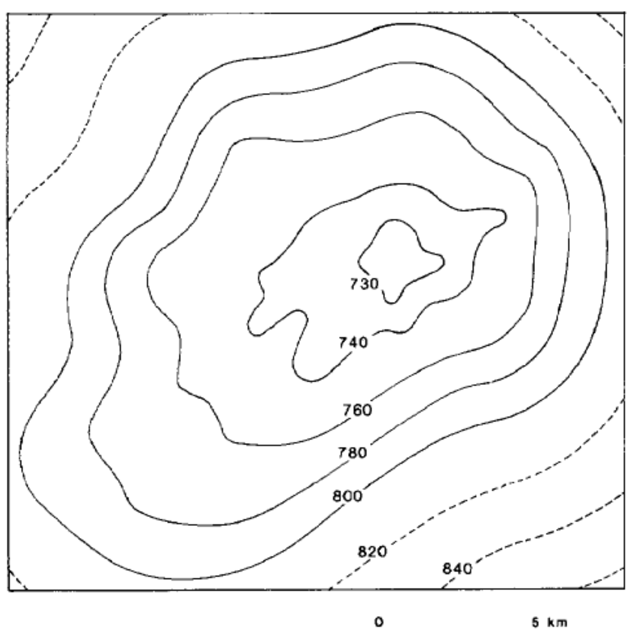

Figure 30 – Contour map of Messoyakha Gas Field (Sapir et al., 1973)

The structural enclosure of the field is 84 meters and the aerial extent of the field is 12.5 km x 19 km (Makogon et al., 2005). A contour map of the top of the Cenomanian Dolgan Formation at Messoyakha is shown in Figure 30 (Krason and Finley, 1992). The depths refer to the depths (in meters) below mean sea level. Figure 31 shows the cross sectional views of Messoyakha as published in (Makogon et al., 1971a).

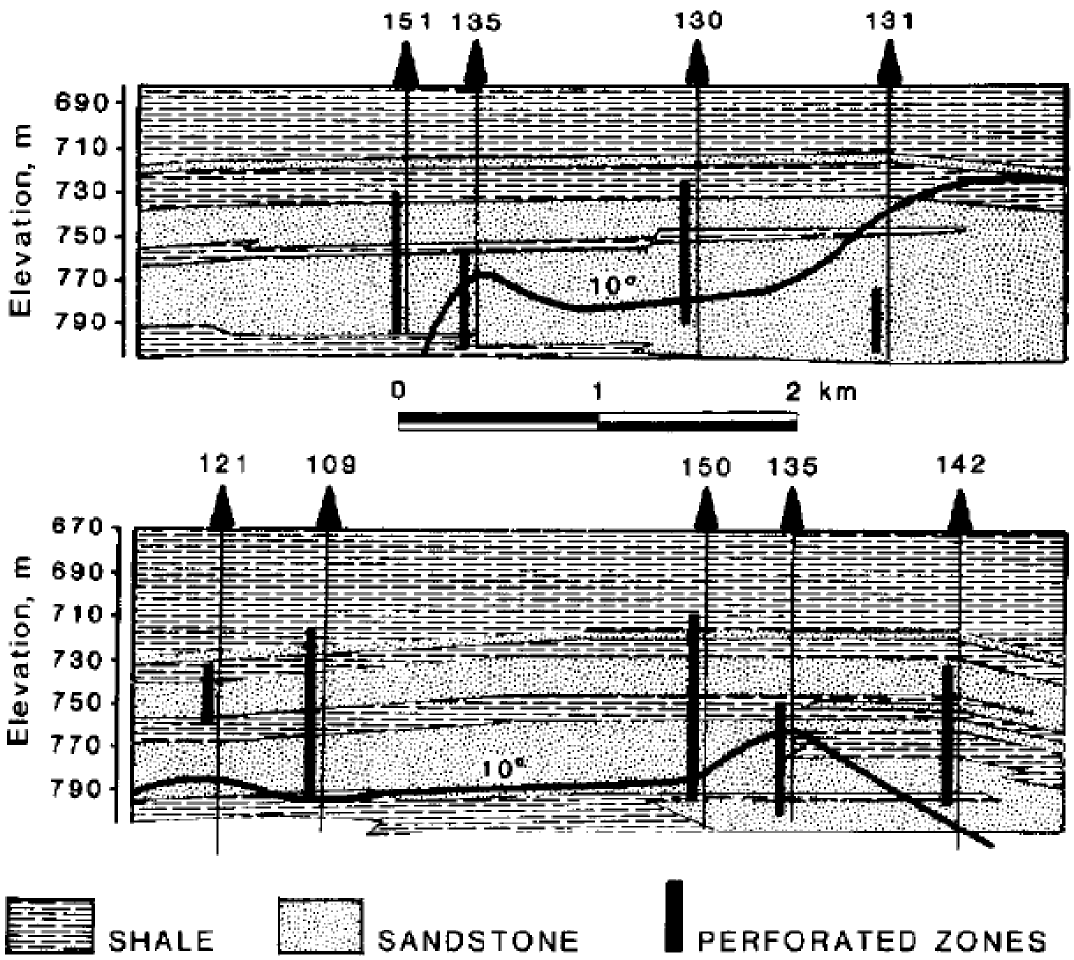

Figure 31 – Cross sections of Messoyakha reservoir (Makogon et al., 1971b)

These figures show the 10°C isotherm which is inferred as the base of the hydrate stability zone.

More than 60 wells have been drilled in this field with spacing of 500 m x 1000 m. Production began in 1970 and continued until 1977. Initial production per well was reported to range from

111 MSCF/D to 6275 MSCF/D. The field was shutdown from 1979-82. During this shutdown period the reservoir pressure increased due to the continued dissociation of hydrates. The pressure was restored to the equilibrium pressure during the shutdown and then the gas production was again started at lower flow rates. Figure 32 shows the reservoir pressure behavior and the gas production respectively. From the Figures it can be seen that when the flow rates were returned to zero at Messoyakha, the average pressure kept on increasing. It was interpreted that gas released by hydrate dissociation led to the recharging of the free gas reservoir.

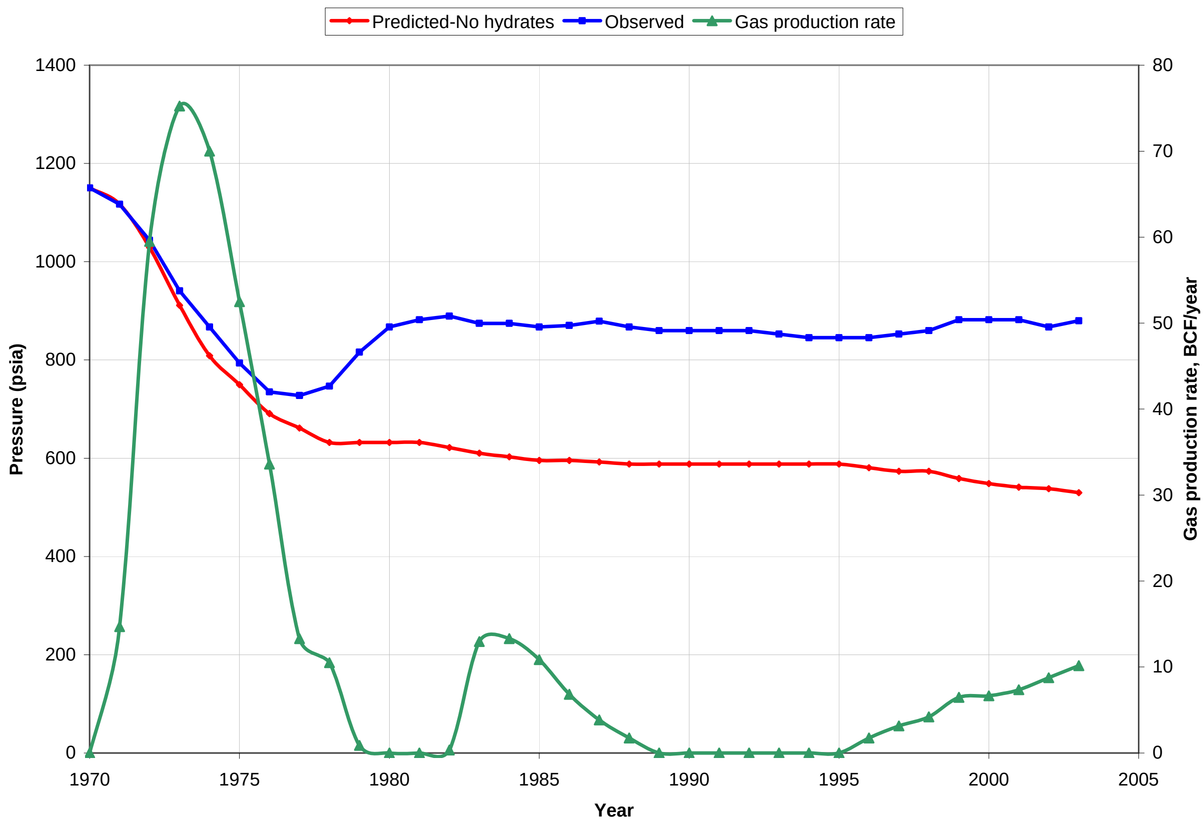

Figure 32 – Production behavior at Messoyakha (Makogon et al., 2005)

Messoyakha gas field has been described as a hydrate capped gas reservoir i.e. the upper portion of the reservoir contains gas in hydrate state (Makogon et al., 1971a; Makogon et al., 1970) and the lower portion of the reservoir contains free gas. Messoyakha is actually divided into two portions; upper portion which lies in the thermodynamically stable hydrate zone and the lower portion which lies outside the hydrate stability zone. It should be noted that the boundary between upper and lower portion is not lithlogical but thermodynamic. In the upper portion, hydrates are stable and in the lower portion they are unstable and hence absent. There has been not enough information in the literature about the exact percentage of reservoir portion filled with hydrates. Initial hydrate saturation is described to be about 20% (Makogon et al., 2005).

The estimated volumetric gas reserves at Messoyakha range from 1.3 to 14 tcf (Krason and Finley, 1992). Figure 33 shows the reserve estimates at Messoyakha by various sources (adapted from (Krason and Finley, 1992)). Uncertainty also exists for the gas in hydrate form at Messoyakha gas field. (Sheshukov, 1973) calculated that 2.2 tcf of gas was in hydrate form in upper portion of Messoyakha and 0.6 tcf of gas was present as free gas in lower portion of Messoyakha. Recently, (Makogon et al., 2005) reported that initial in-place gas (free-gas) at Messoyakha was 848 BCF and the producible reserves from hydrate state were 424 BCF.

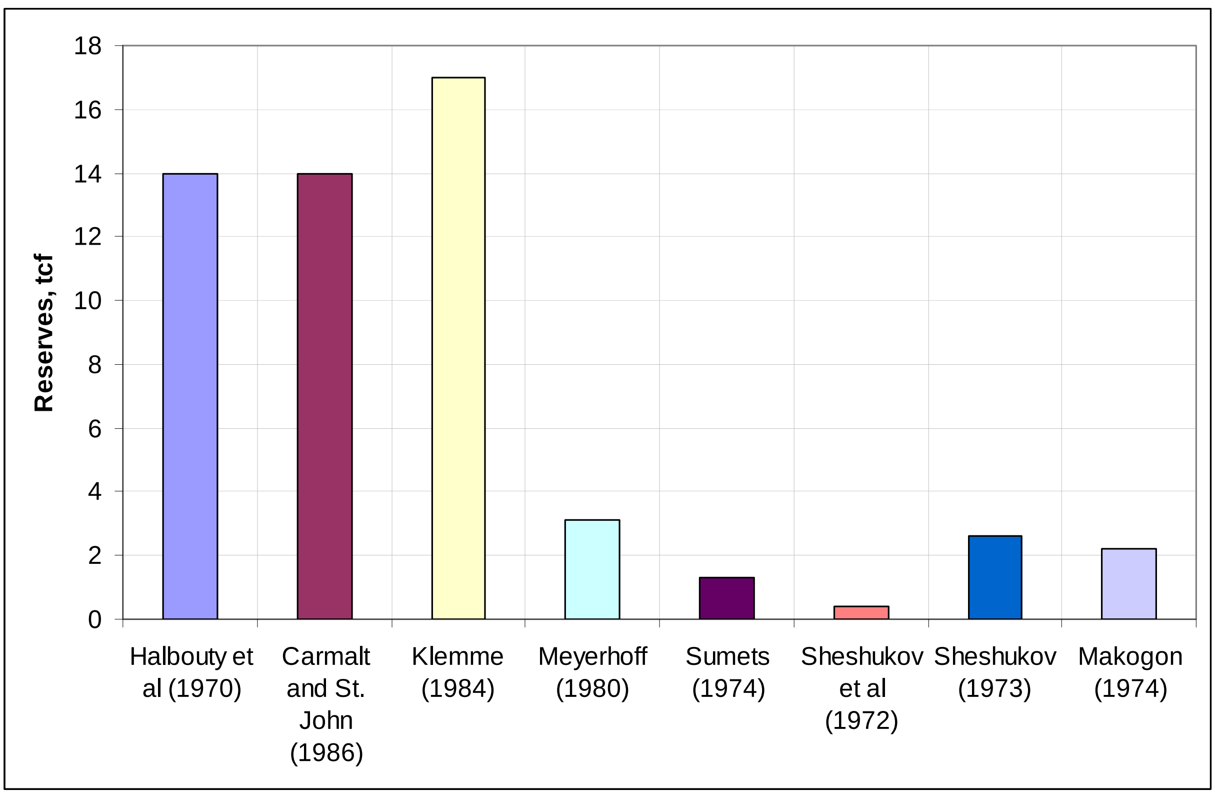

Figure 33 – Various estimates of gas-in-place at Messoyakha (Data from (Krason and Finley, 1992))

The production rates from the wells which were perforated in the hydrate portion i.e. upper portion of the reservoir were much less than the wells which were perforated in the deeper free gas portion of the reservoir. When the depressurization occurred in the hydrate layer, it caused the hydrates to dissociate. When the gas hydrate dissociates, the temperature in the nearby formation decreases. The water and gas produced by dissociation again react together to form secondary hydrates near the well, and hence plug the perforations. On the other hand, the depressurization that occurs in the lower free gas portion of the reservoir is away from the equilibrium conditions. Therefore, the wells completed in the deeper free gas zone were able to operate at high flow rates. Table 2 gives the gas production from selected wells according to perforations at different intervals (Makogon et al., 1971a).

Table 2. Production from various perforation locations (Makogon et al., 1971b)

Well No.	Proportion of perforation in hydrate zone	Distance from perforations to hydrate-gas interface (m)	Production rate (1000 m^3/D)
121	100	+64	26
109	100	+6	133
150	81	-6	413
131	0	-59	1000

Some of the wells which were completed in the hydrate zone were stimulated by using chemicals such as calcium chloride and methanol. These chemicals are inhibitors for hydrate formation, or in other words, make the hydrates unstable by changing the equilibrium curve. This chemical stimulation destabilized the hydrates resulting in melting of hydrates near the well. After stimulating the wells, it was possible to operate the same wells at higher wellhead pressures. Figures 34 and 35 (Makogon et al., 1971a) demonstrate the data of treating two of the wells with methanol.

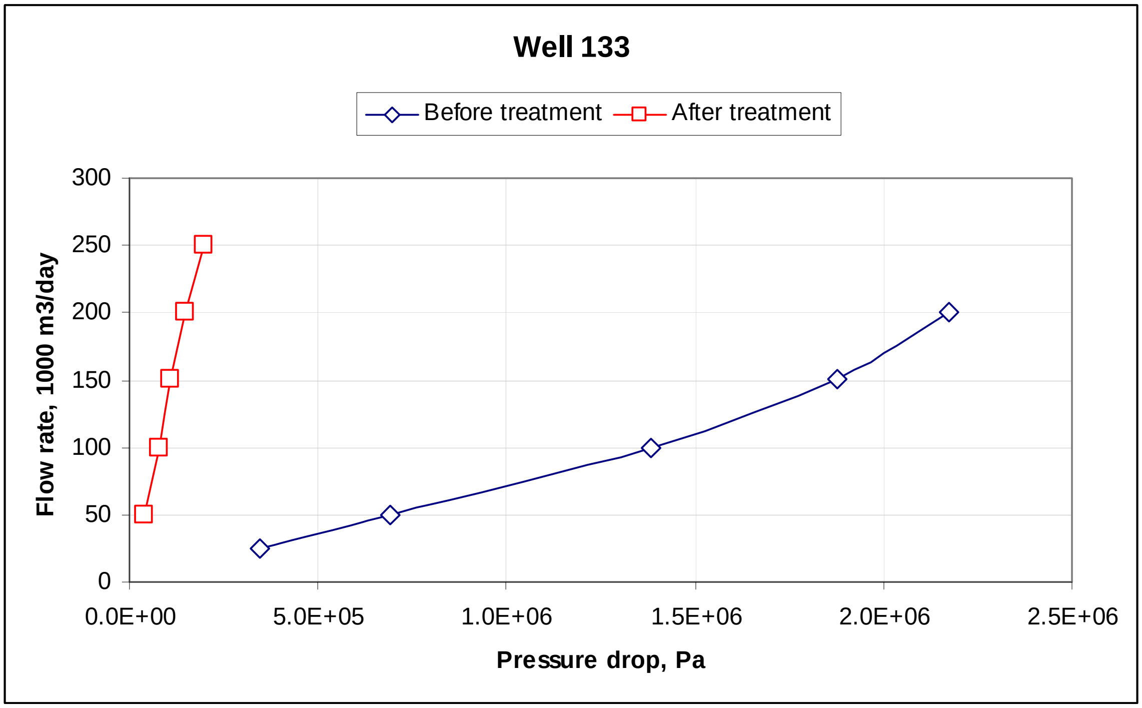

Figure 34 – Effect of chemical stimulation for Well 133 (Makogon et al., 1971a)

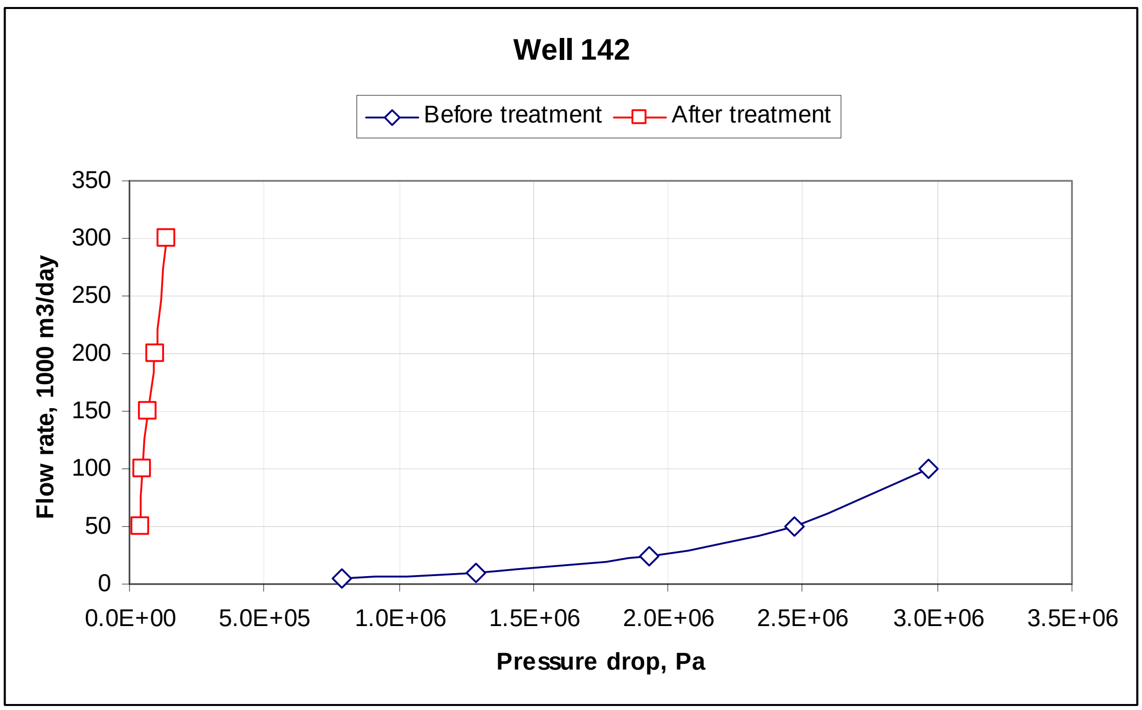

Figure 35 – Effect of chemical stimulation for well 142 (Makogon et al., 1971a)

There is not a consensus on the depth of the gas-water contact (Krason and Finley, 1992). Table 3 shows the gas-water contact information published by three groups. According to Makogon, the gas-water contact has not moved during the entire period of gas production (Makogon, 2007; Makogon et al., 2005).

Table 3. Gas/water contact values

Source	Gas/water contact
(Meyerhoff, 1980)	-805 m
(Makogon, 1984, 1988; Makogon et al., 2005)	-819 m
(Sapir et al., 1973)	-779 to -811 m

Rock properties at Messoyakha are highly heterogeneous. The range of the rock properties, their average values, geothermal gradient and initial reservoir pressure are given in the Table 4.

Table 4. Reservoir properties (Makogon et al., 2005)

Property	Range
Porosity	16-38%
Permeability	10 to 1000 md
Geothermal gradient	4.2 °C/100m
Residual water saturation	29 to 50%
Initial reservoir pressure	1150 psia

Details concerning Messoyakha are published in various sources (Krason and Ciesnik, 1985; Krason and Finley, 1992; Makogon et al., 2005; Makogon et al., 1971a; Meyerhoff, 1980). We refer the reader to these sources if one is interested in knowing more of the detail surrounding the Messoyakha gas reservoir.

The only data available on the saturations of water, gas and hydrates in the respective zones i.e. upper hydrate zone and the lower free gas zone is from (Makogon et al., 2005). Average water saturation was described to be 40%, salinity to be 1.5%, Initial hydrate saturation to be 20%. Using this information, the upper and lower portion of the reservoir contain the saturations as described in Table 5

Table 5. Average saturations at Messoyakha (Makogon et al., 2005)

Saturations	Hydrate layer	Free gas layer
$S_{hydrate}$	20	0
S_{water}	40	40
S_{gas}	40	60

However, there is an important point to be noted here. If the above saturations exist during the initial state of the reservoir, the hydrodynamic pressures should exactly follow the equilibrium pressures at each depth. This phenomenon can be explained using the schematic in Figure 36

If the geothermal gradient exists in the hydrate layer, it will then cross the equilibrium curve which is actually a three phase layer. At the three phase layer, the hydrodynamic pressure is equal to the equilibrium pressure. For large thicknesses, the three phases can not exist throughout the reservoir because it will mean the pressure will follow the equilibrium curve. If the pressure follows the equilibrium curve, the geothermal gradient will no longer be a single value but in fact continuously changing.

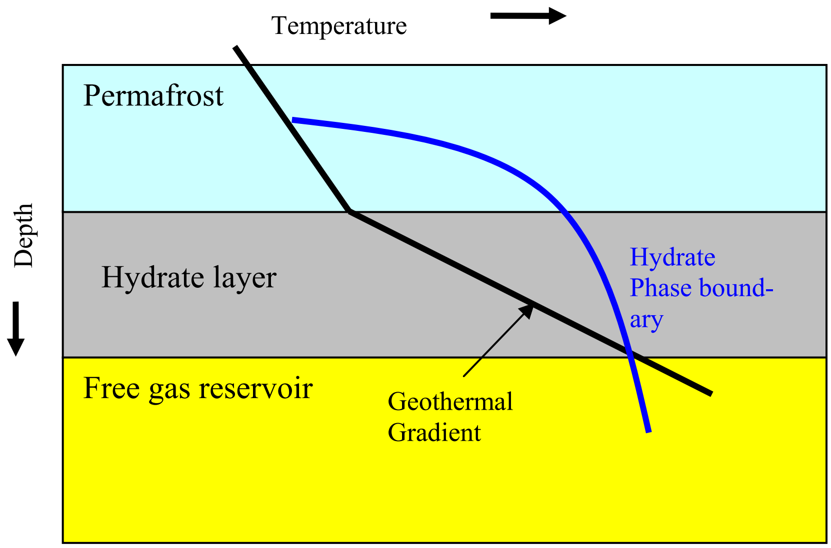

Figure 36 – Hydrate stability zone

It should be pointed that there is a dearth of information on the effect of porous media on hydrate equilibrium behavior and it is not understood fully. Moreover, there is little or no information available on the capillary pressures and relative permeability in presence of hydrates at Messoyakha. It might very well be possible that the co-existence of all the three phases is affected by capillary pressures, and the effect called self-preservation of natural gas hydrates. Given these constraints, this problem was simplified by assuming that in the hydrate layer there is hydrate and gas and in the lower free gas layer, gas and water. This simplification was necessary to initialize the model which will be discussed in the later section.

As demonstrated in Figure 33, there has been an uncertainty about the estimated reserves at Messoyakha. Volumetric calculations were done using the contour map provided for Messoyakha (Makogon, 2007). For ease of volumetric calculations, the ellipsoid contours were first transformed into circular contours. Using this methodology the radius of the deepest contour was found to be 7,648 meters. Using this radius and the reservoir depths as defined in (Makogon et al., 2005), the gas in place in hydrate form and as free gas was calculated. Using the geometry described in (Makogon et al., 2005), the in-place gas reserves (both as hydrate and as free gas) was 5-7 times greater than that published. Moreover, there was not enough information on the production from different wells drilled throughout the life of the reservoir. In our calculations, we assumed the structural enclosure to be same as published i.e. 90 meters. The top 50 meters was supposed to be inside the hydrate stable region and the lower 40 meters was outside the hydrate stable region.

The sources that we have referred to for collecting the information on Messoyakha reservoir cite (Makogon, 1974) for the description of the reservoir rock and fluid properties. There are large variations in the rock properties i.e. porosity, permeability and only average properties have been described. There is no information on the porosity and permeability distributions at Messoyakha in the open literature. The salinity is defined as maximum of 1.5%. This salinity is of course less than the typical pore water salinity in the offshore sediments. However, this salinity value can also alter the phase equilibrium curve of gas and water. Gas composition at Messoyakha consists of major amount of methane and other minor constituents (Makogon et al., 2005). Table 6 describes the gas composition at Messoyakha (Makogon et al., 2005).

Table 6. Gas composition at Messoyakha

Gas	Percentage
CH_4	98.6
C_2H_6	0.1
C_3H_8	0.1
CO_2	0.5
N_2	0.7

In essence, the situation here pertains to the data limited system. Data provided in various sources does not agree with our calculations and basic reservoir engineering principles. Hence any efforts to run a full field model of Messoyakha were dropped. Instead, we proceeded with building a range of 2-D cross sectional models representative of Messoyakha. Figure 37 shows the model geometry which is used for the simulation work.

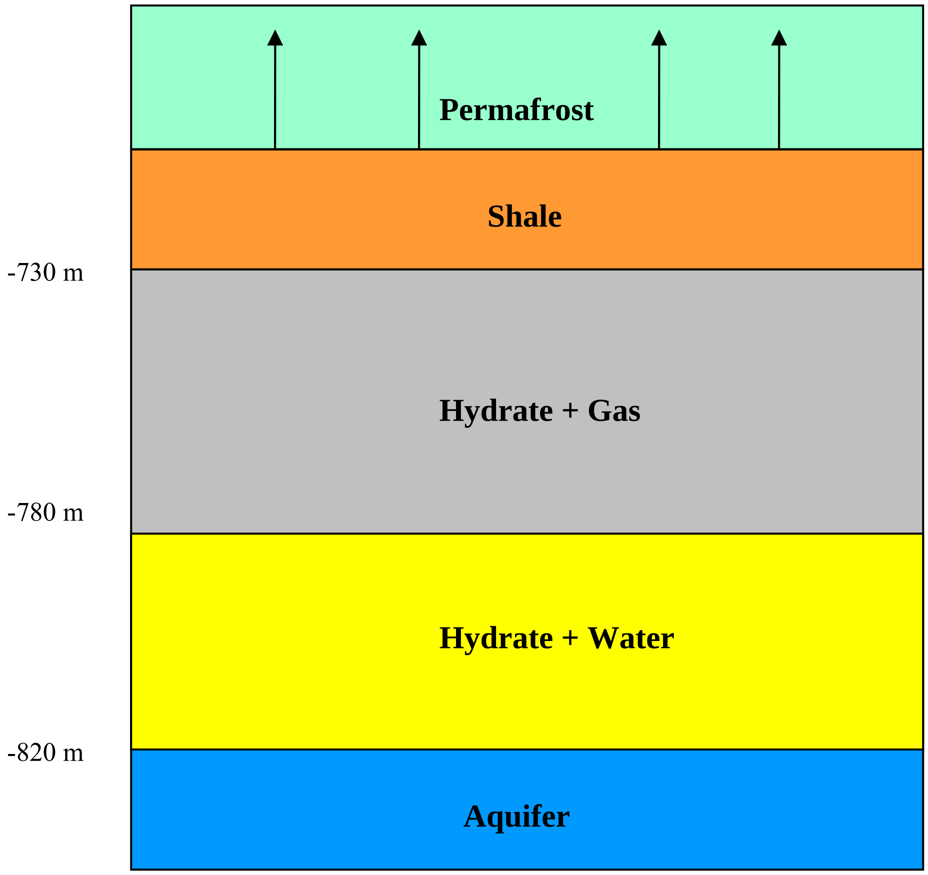

Figure 37 – Representative geometry of Messoyakha Reservoir

TOUGH+Hydrate Simulator

TOUGH+Hydrate is a numerical simulator developed by (Moridis et al., 2005) at Lawrence Berkeley National Laboratory, USA. TOUGH+Hydrate can simulate the behavior of hydrate bearing porous media. Some salient features of this simulator are

- Capability of modeling non-isothermal gas release by hydrate dissociation
- Heat transfer in porous media
- Option of hydrate reaction as both equilibrium and kinetic
- Can handle any combination of possible hydrate dissociation mechanisms i.e. depressurization, thermal stimulation and inhibitor injection
- Tracking of gas released by hydrate dissociation in reservoir

Using this simulator, a number of studies have been carried out for simulating gas production from hydrate reservoirs under different geologic conditions (Moridis, 2003, 2004; Moridis and Collettt, 2003, 2004; Moridis et al., 2004; Moridis and Kowalsky, 2005; Moridis and Sloan, 2007). These studies have served as building blocks for my modeling work of Messoyakha.

Fig. 39 shows the 2 Dimensional, R-Z model used to simulate gas production from Messoyakha. Fig. 40 presents the 2 Dimensional grid system.

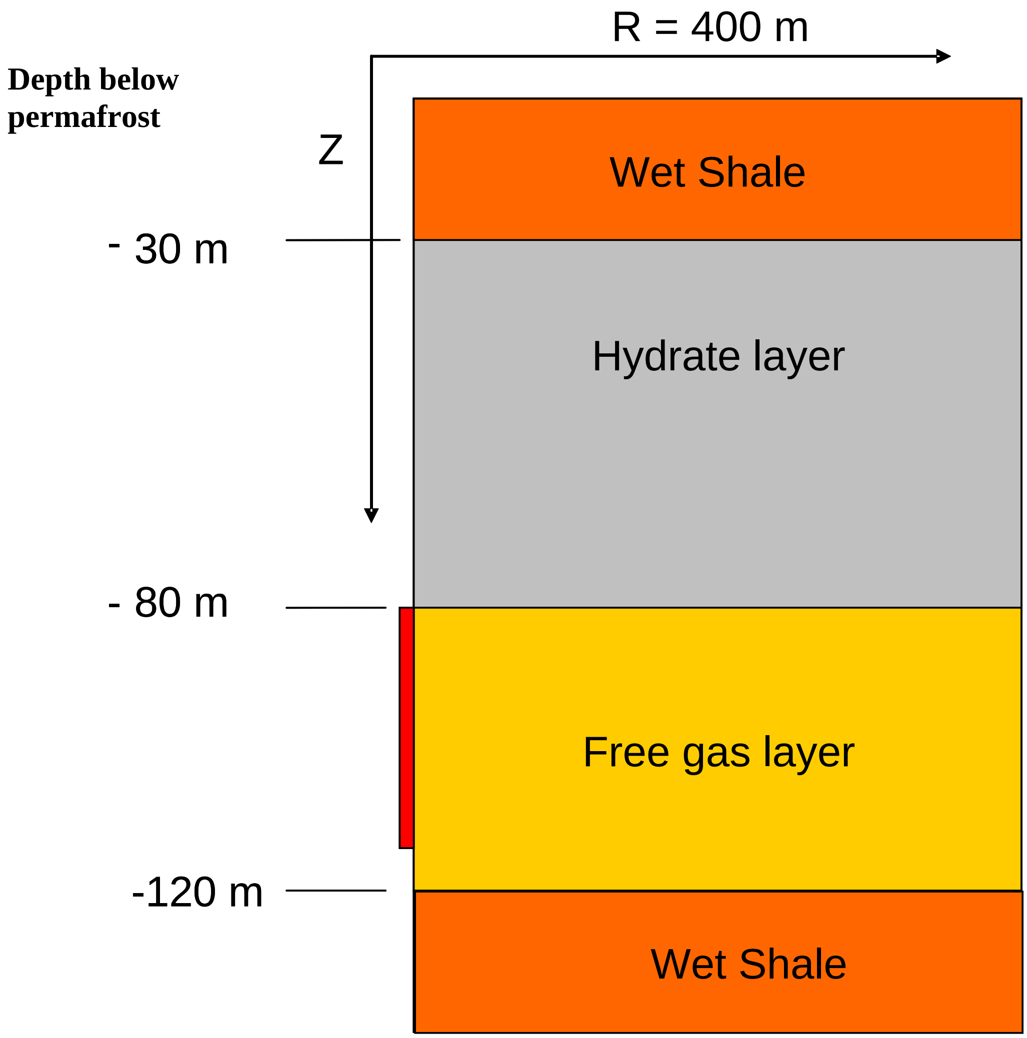

Figure 39 – Schematic of model set-up (base case) in TOUGH+Hydrate

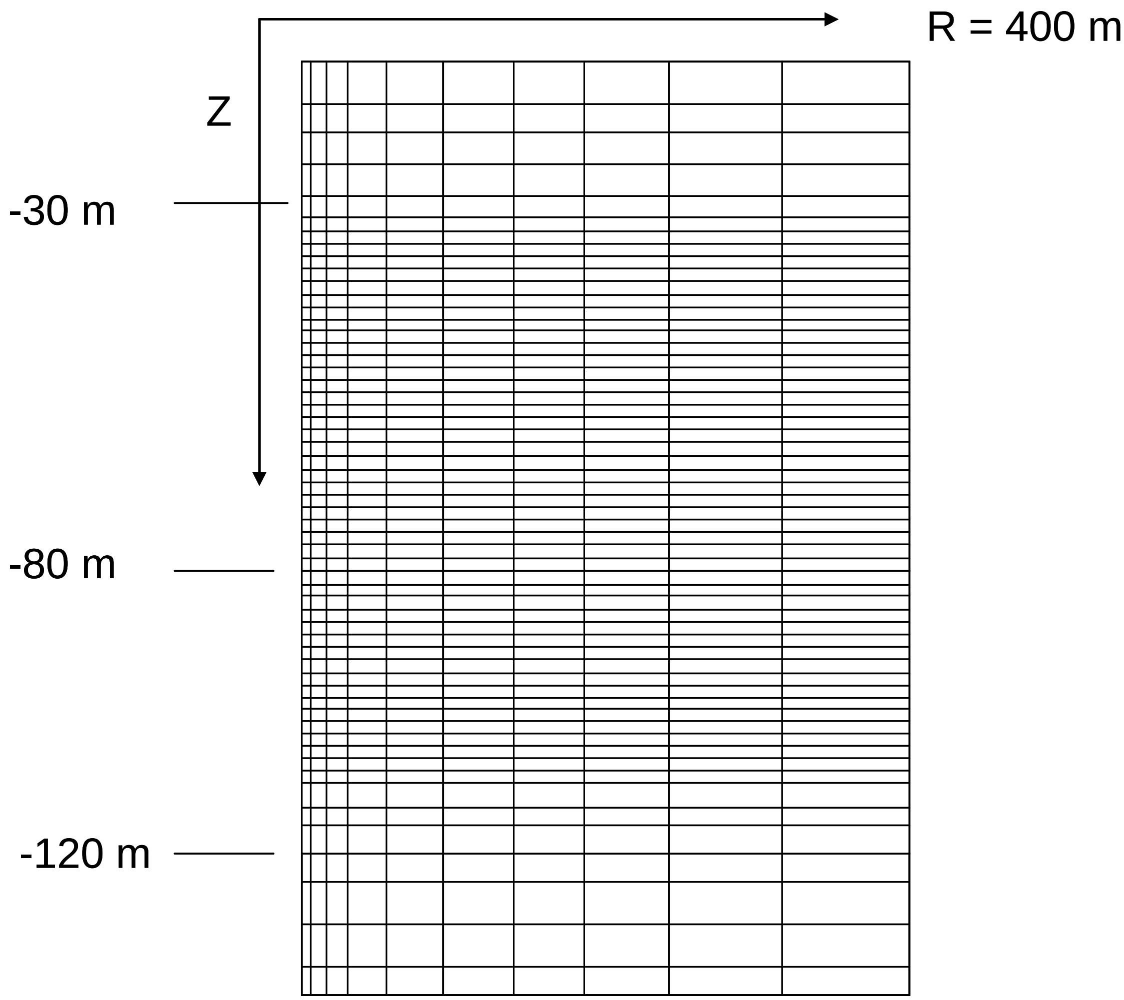

Figure 40 – Grid system for base case using TOUGH+Hydrate

This model was then discretized into 100 radial elements and 135 layers (Figure 40). This fine scheme is necessary to capture the saturation changes occurring in hydrate layer and close to hydrate layer. Hence there are a total of 13500 elements. The methodology followed in simulating Messoyakha is as follows.

1. Build a base case based on previous simulation experience of hydrates
2. Keep changing the properties and scenarios to test for various field observations at Messoyakha.

Based on this methodology we started with base case with properties in Table 7.

Table 7. Base case properties

Property	**Hydrate layer**	**Free gas layer**
Porosity	0.35	0.35
Absolute permeability, md	500 md	500 md
Thickness	50 m	40 m
Hydrate saturation, Sh	0.5	0
Gas saturation, Sg	0.5	0.5
Water saturation, Sw	0	0.5
Irreducible water saturation	0.28	0.28

The reason to start off with this base case was to analyze the primary results and then construct a range of 2-D models to test various observations at Messoyakha. This approach eventually led us to a detailed parametric study for a hydrate capped gas reservoir in general.

Before running any numerical model, it is very important to initialize the data set. This is because whatever perturbation (i.e. production, heating, etc.) is to be studied, all the model parameters should respond to only that perturbation. Initialization process in TOUGH+Hydrate is a challenging task.

The following assumptions were made to initialize the model

- Salinity was assumed to be zero. Since the upper portion of the reservoir is set-up as gas and hydrate, there is no provision to define salinity in this type of system. In other words, neither the “gas phase” nor “hydrate phase” can account for salt.
- Initial pressure at the hydrate-gas interface is 7.92e6 Pa (1150 psia). This pressure is representative of the pressure at the Messoyakha. Based on this pressure, the temperature is about 10.88 °C (for 3-phase methane-hydrate-water) equilibrium. This temperature is close to 10°C isotherm defined in (Makogon et al., 2005).

The initialization process involves finding correct pressures and temperatures along a single column. This column was broken down into two separate columns i.e. hydrate column and the lower free gas column. Knowing the pressure and temperature at the interface, and using the geothermal gradient of 0.042 °C/m, the temperature and pressure distribution in the hydrate column was calculated. This resulted in a heat flux value in the hydrate zone.

The temperature in the bottom of free gas zone was changed to obtain the same heat flux value as that in hydrate zone. Then these two columns were then connected. This is then the initialized condition of the model. (Moridis and Kowalsky, 2005) explain the initialization process in extreme detail.

Once the model is initialized, it is ready to be simulated for gas production. Figure 41 shows the initial state of the model. It can be compared with Figure 28.

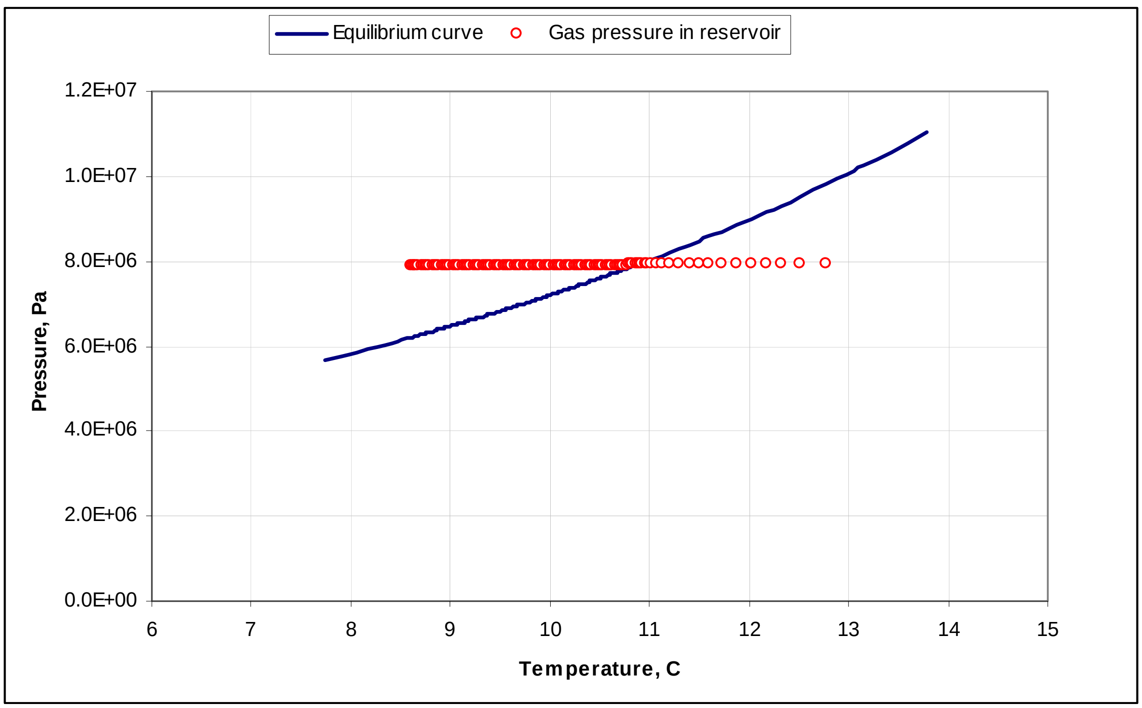

Figure 41 – Initial Thermodynamic State of Messoyakha

There is a minor difference in equilibrium pressure and temperature at the interface between my model and actual published data on Messoyakha. The reason for this is that initial pressure of

1150 psia (7.92e6 Pa) was assumed at interface. This pressure gives the equilibrium temperature of 10.88 °C.

The production from this 2-D model was at constant flow rate of 170,000 Sm^3/Day (6 MMSCF/Day). The well was completed in free gas layer with the production grid block right at the interface of hydrate zone and free gas zone. The thickness of the reservoir in free gas which was perforated was 16 meters. The following table gives the production parameters used in the model run.

Table 8. Production parameters for base case

Production parameter	**Value**
Flow rare	170,000 Sm3/Day
Perforated interval	16 meters
Distance of perforation from interface	0.5 meters

Moridis and Kowalsky (2005) introduced the concept of "Rate replenishment ratio (RRR)" and "Volume replenishment Ratio (VRR)" for production from Class 1 hydrate deposits. These two are defined as follows:

$$\mathrm{RRR} = \frac{\text{Rate of } \mathrm{CH_4} \text{ released by hydrate dissociation}}{\mathrm{CH_4} \text{ production rate at the well(s)}}$$

$$\mathrm{VRR} = \frac{\text{Cumulative gas released from hydrates}}{\text{Cumulative gas production at the well(s)}}$$

For each run, we have reported four different results

- Evolution of pressure gradient at different times
- Evolution of temperature gradient at different times
- Pressure-Temperature regime of the reservoir at different times
- RRR
- VRR

Base case is run for 8 years of constant rate production and the shut down for next 3 years. The results are shown in Figures 42-46. In Figure 42, pressure in the reservoir (gas phase pressure) is recorded at different times during the simulation runs. It is seen that as soon as the production continues, the gas pressure gradient in the hydrate layer is the same as that in the free gas layer. If we take a look at the Figure 43, the temperature in the reservoir continues to decrease because of dissociation of the hydrate.

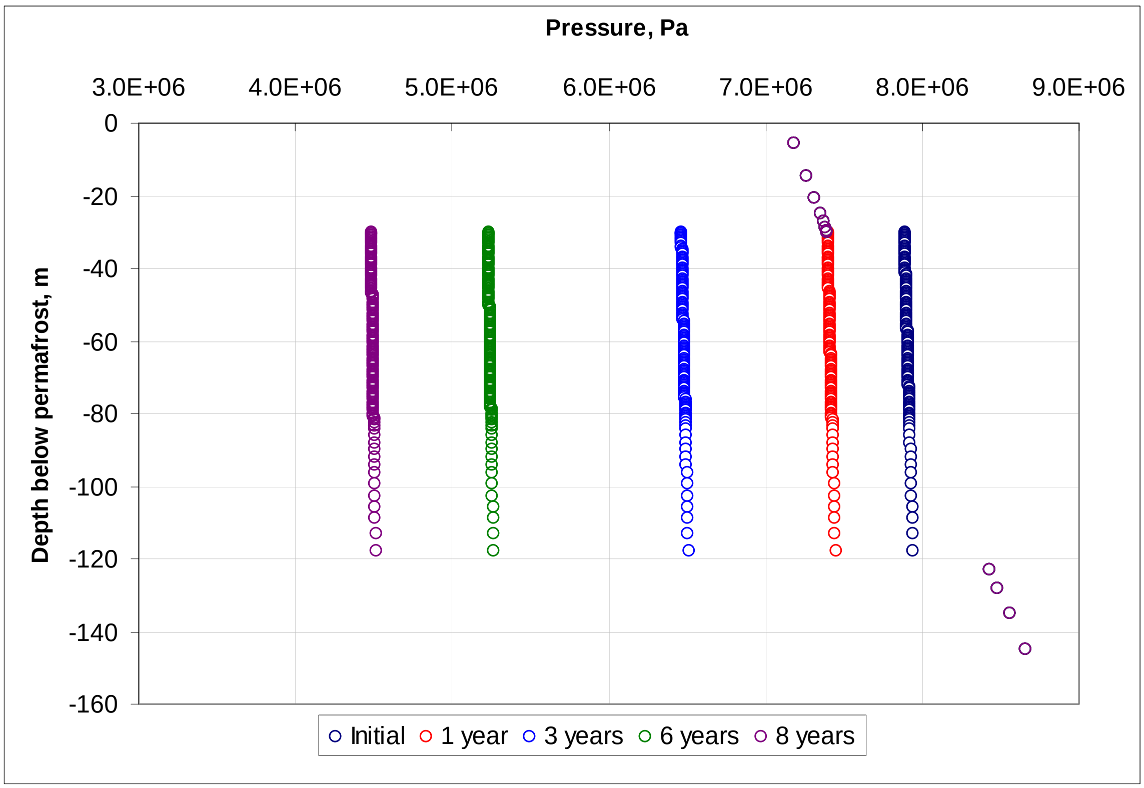

Figure 42 – Pressure evolution over time for base case

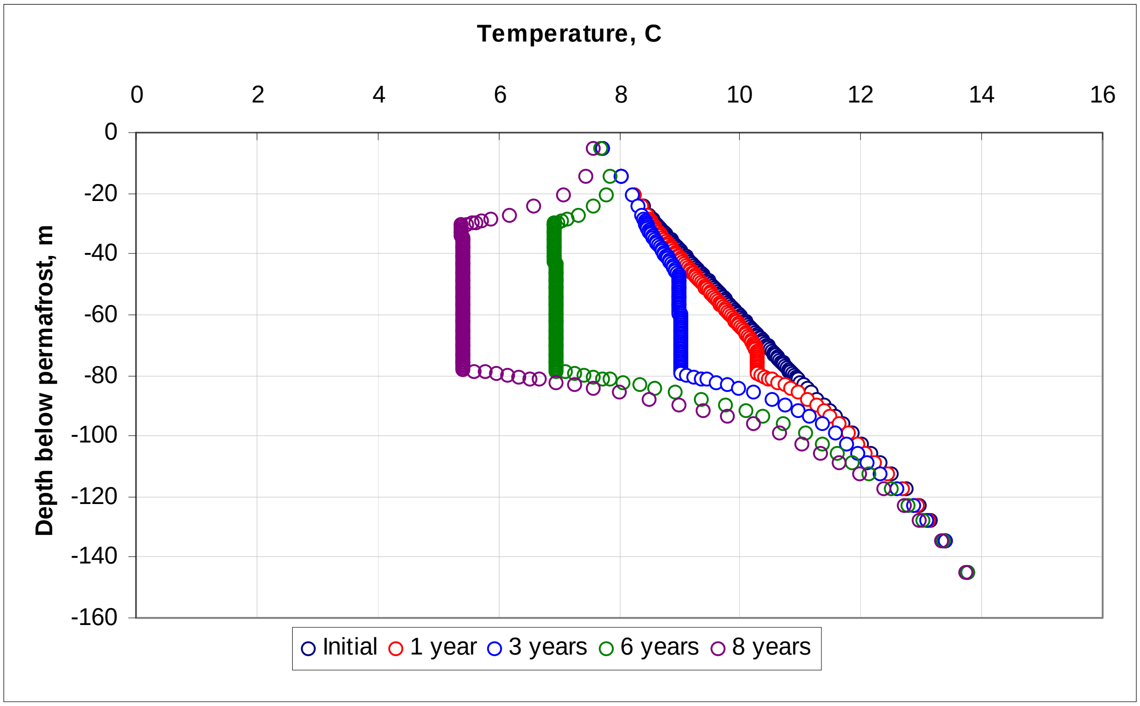

Figure 43 – Temperature evolution over time for base case

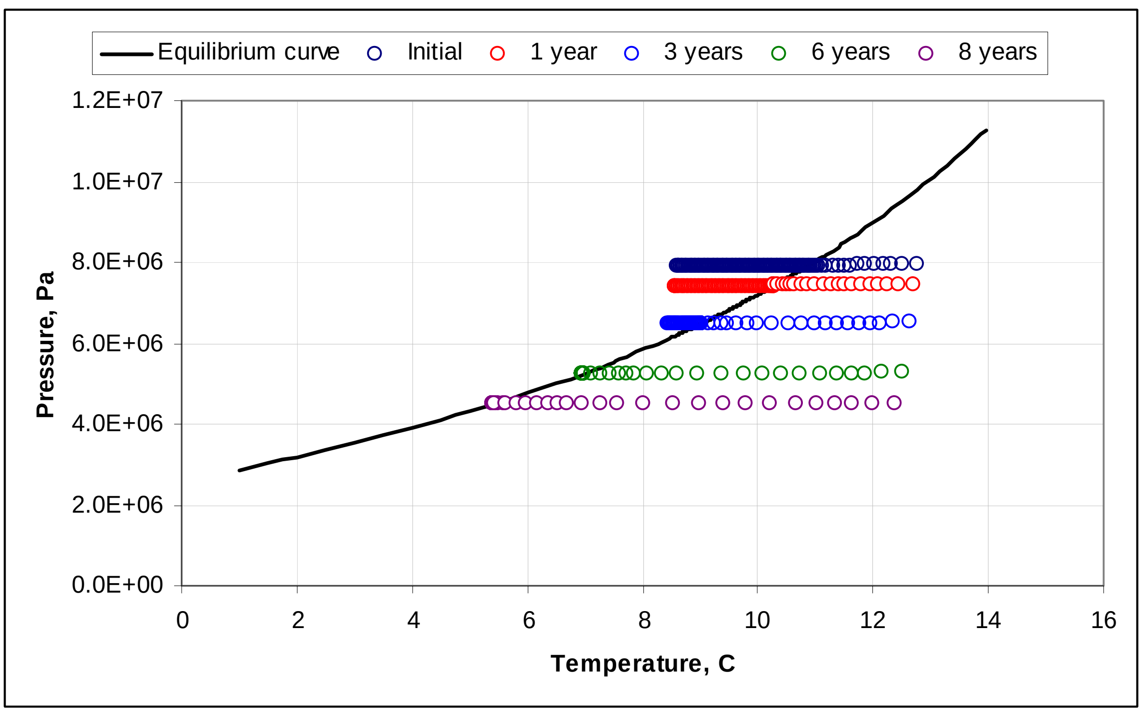

Figure 44 – Pressure-Temperature trace for base case with time

Since the hydrate dissociation is an endothermic process, this transfers the heat from the surrounding rock. Figure 44 is actually the combination of the Figures 42 and 43, and actually describes the driving forces in a hydrate reservoir. From Figure 44, it is seen that the top of the hydrate layer enters dissociation regime after about 4 years of production and then the entire hydrate layer is under the depressurization driving force.

Figure 45 presents the 'Rate replenishment ratio' for the base run. In Figure 46, we present the 'Volume replenishment ratio'. These two graphs clearly show that over 30% of the gas produced from the free gas layer at Messoyakha over the years has been coming from the gas hydrate layer.

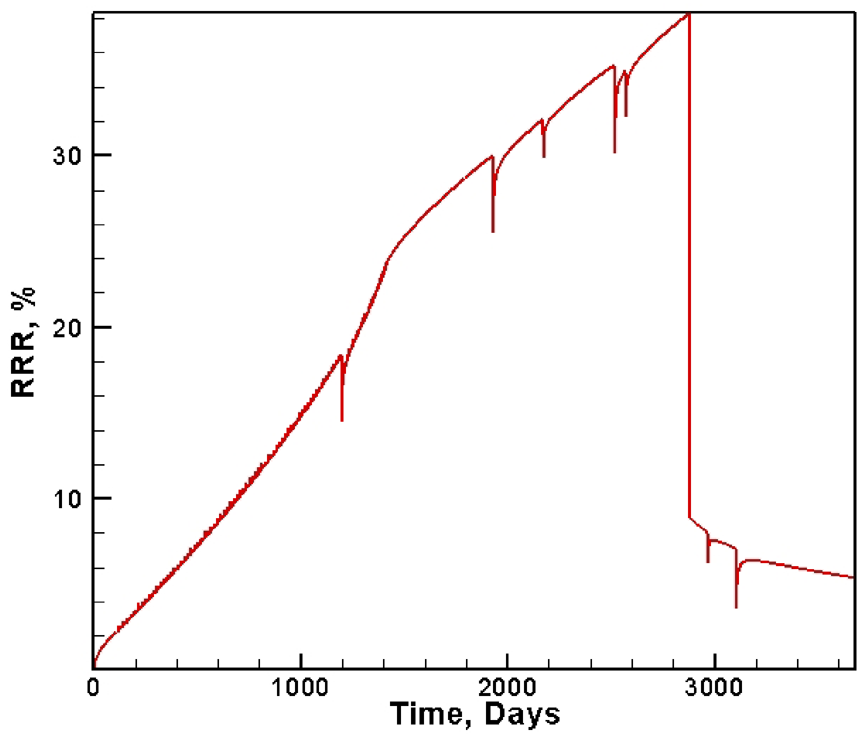

Figure 45 – Rate replenishment ratio for base case

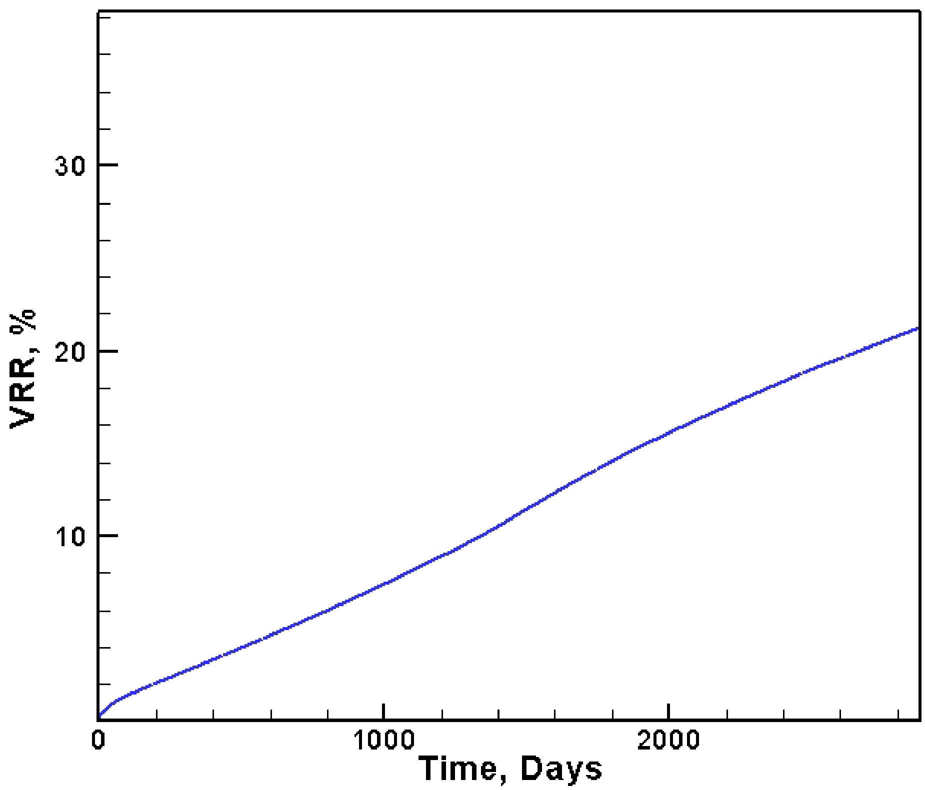

Figure 46 – Volumetric replenishment ratio for base case

Effect of Permeability in the Gas Hydrate Layer

Since the permeability of the gas hydrate layer is unknown, we made a series of computer runs varying the permeability of the gas hydrate layer using the values shown in Table 9.

Table 9. Hydrate layer absolute permeability

Parameter	**Value(s)**
Absolute permeability-Hydrate zone	0.01 md 0.1 md 1 md

Using these parameters, the average pressure in the free gas layer is plotted as a function of time. The average pressure in the free gas layer increases when the well is shut in. The hydrates experience the higher pressure differential caused by higher depletion rate in the free gas zone as compared to that in the hydrate zone. This is similar to the pressure behavior observed at Messoyakha field. Figure 47 shows the gain of the pressure from the pressure at the time of shut-in.

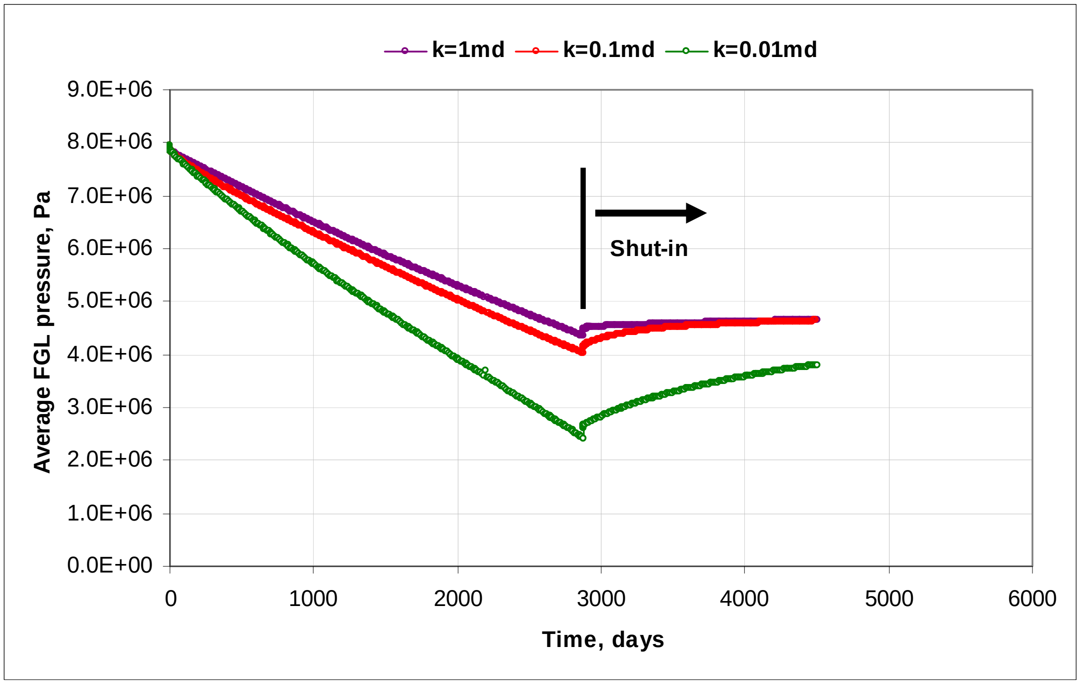

Figure 47 – Pressure increase in the free gas layer due to hydrate dissociation

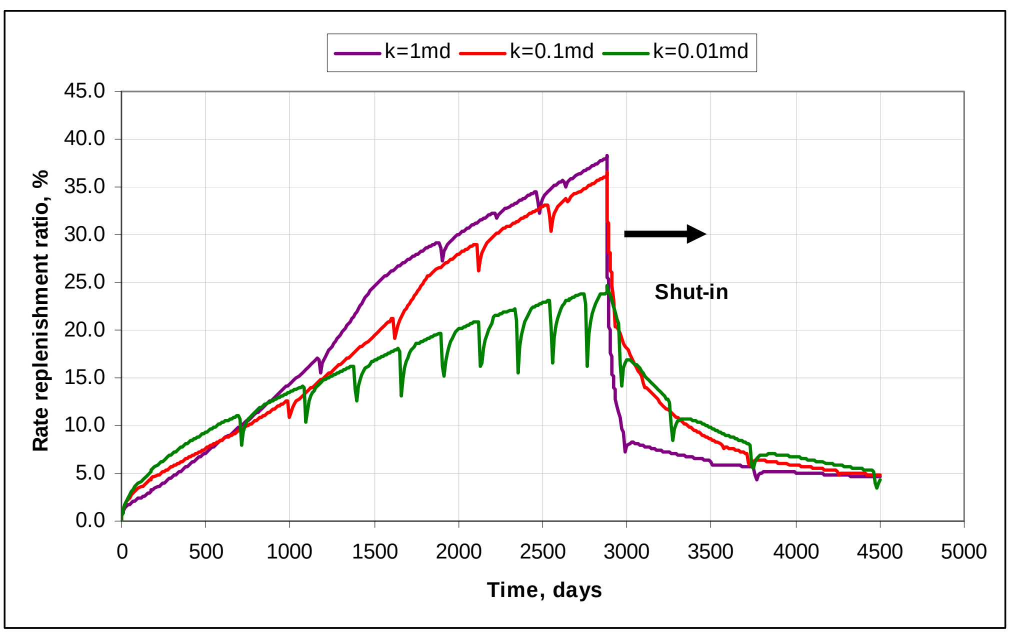

Figure 48 – RRR for different hydrate layer absolute permeability values

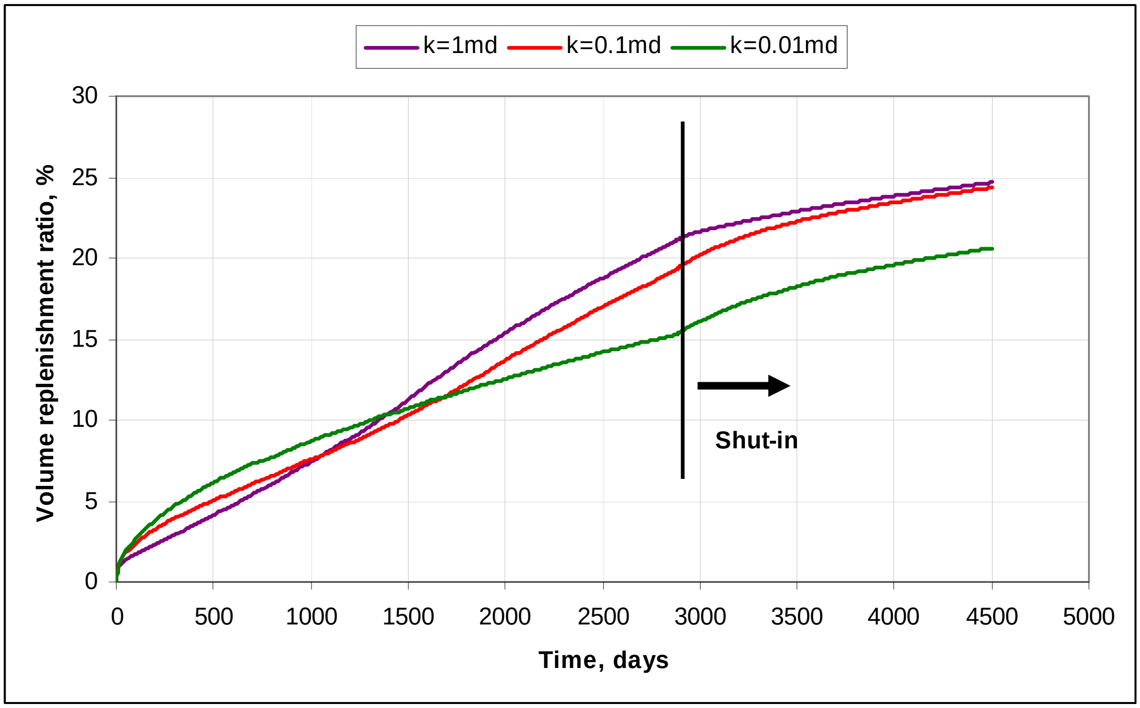

Figure 49 – VRR for different hydrate layer absolute permeability values

There are very few publications which discuss the decrease in the absolute permeability of the porous media when impregnated with hydrates. This reduction in absolute permeability has an important effect on the gas production from hydrates i.e. contribution to the overall production and reservoir pressure behavior, as illustrated in Figures 48 and 49. Figure 48 shows the comparison of "RRR" for different permeability values. Figure 49 shows the VRR for different permeability values. As the permeability in the hydrate bearing formation decreases, the period pressure in the free gas layers increases more during shut-in, because there is a larger pressure differential between the free gas layer and the hydrate layer.

The model was run just as in base case for 8 years of production, followed by 3 years of shut-in with hydrate layer permeability of 0.1 md. Figures 50-52 show the various results for this case. Comparing these figures to those of the base case provides important information on the dissociation behavior of hydrates during depressurization at Messoyakha.

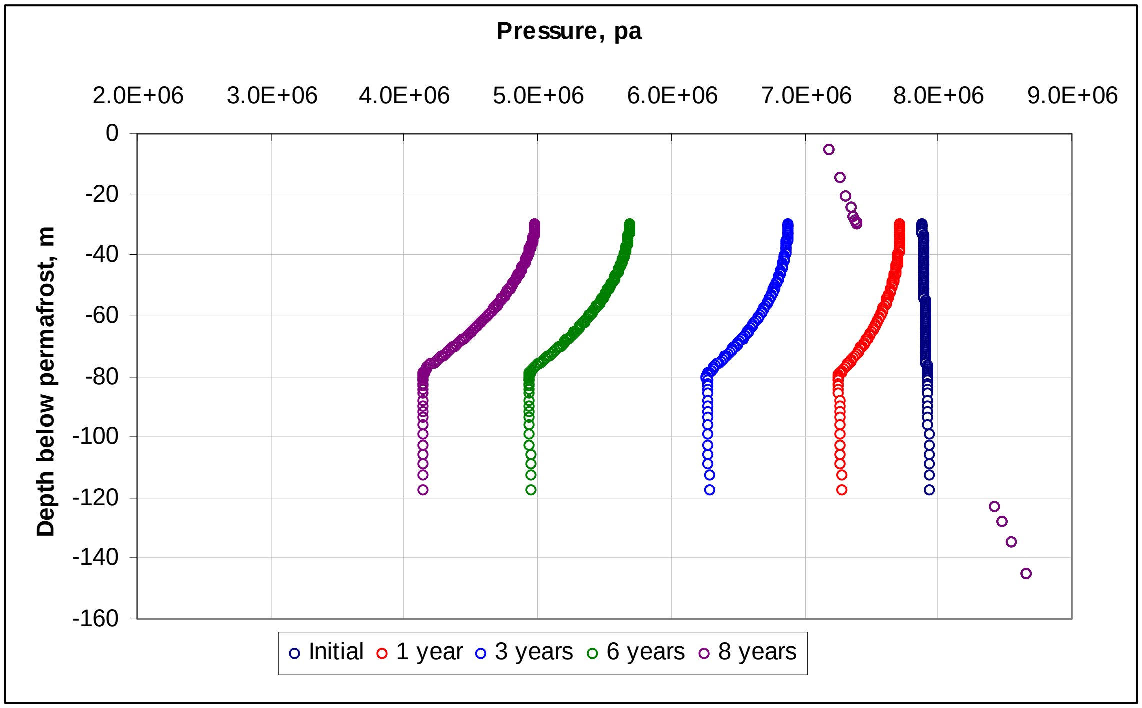

Figure 50 – Pressure evolution with time for hydrate layer permeability of 0.1 md

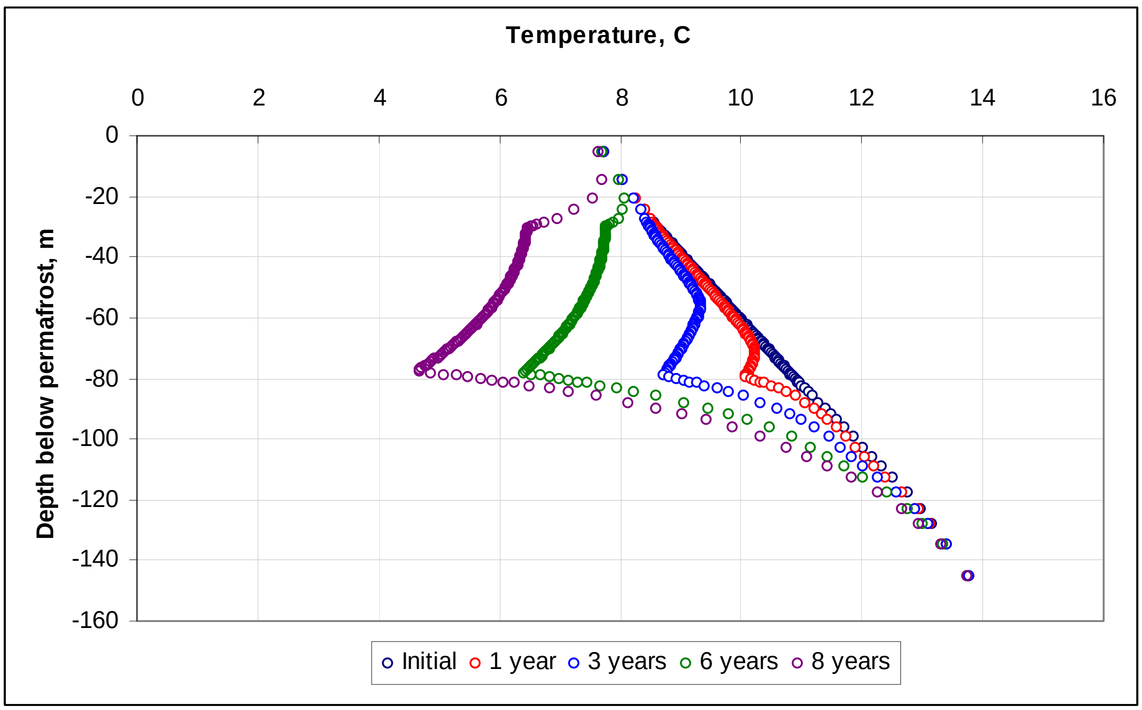

Figure 51 – Temperature evolution with time for hydrate layer permeability of 0.1 md

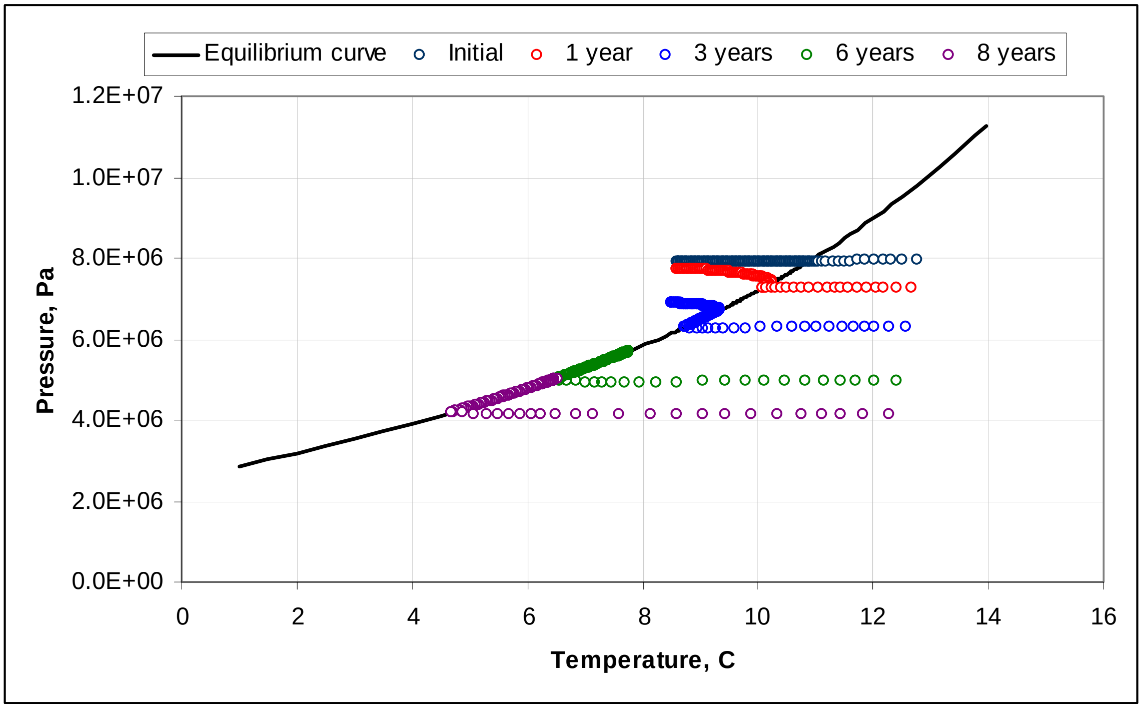

Figure 52 – Pressure –Temperature trace for hydrate layer permeability of 0.1 md

Conclusions

The main objective of this simulation study was to accurately model and explain the pressure observations at Messoyakha Gas Field caused by the production of gas over time. To better understand the mechanisms concerning gas production from hydrates, we constructed a number of 2D cross sectional models to answer as many questions as possible. It is plausible that in the future we may want to simulate the entire field; however at this time, we do not have enough geologic or well data to do so.

We list here important conclusions. Some of the conclusions are based on work that is not included in this summary report, but will be included in a Ph.D. dissertation in early 2008 and in technical papers.

- It is important to know the absolute permeability of hydrate bearing rock for production as well as geomechanical issues. The absolute permeability is a major factor controlling the pressure profile in a hydrate reservoir, to include a hydrate capped gas reservoir. Intuitively, the presence of the gas hydrate will decrease the absolute permeability of the reservoir.

- If the perforations are deep inside the hydrate zone as compared to that in the free gas zone, they can give rise to high pressure drops. This high pressure drop can actually be responsible for sand production.
- In a hydrate capped gas reservoir, the permeability of the free gas zone becomes a limiting factor if the perforations are located near the hydrate-gas interface.
- The pressure increase in the reservoir due to continued hydrate dissociation is an important phenomenon. By shutting-in the well or by producing at lower flow rates may actually maintain the reservoir pressure for long production periods.
- Hydrate saturation has an important effect on gas recovery from Class 1G reservoirs. Lesser the hydrate saturation (and more the gas saturation), the depressurization will be less effective as compared to high hydrate saturation case. This is because the gas is more compressible and hence it has less vigorous pressure wave traveling through it.

6. Bibliography

Collett, T. S., and G. D. Ginsburg, 1998, Gas hydrates in the Messoyakha gas field of the West Siberian Basin - a re-examination of the geologic evidence: International Journal of Offshore and Polar Engineering, v. 8, p. 22-29.

Itasca Consulting Group, 1997. Flac 3d, fast lagrangian analysis of continua in 3 dimensions, Minneapolis, Minnesota.

Jin, G., Patzek, T. W., and Silin, D. B. (2003). Physics-based reconstruction of sedimentary rocks. In SPE Western Regional/ AAPG Pacific Section Joint Meeting, Long Beach, California, USA.

Jin, G., Patzek, T. W., and Silin, D. B. (2004). Reconstruction of sedimentary rock based on mechanical properties. Physical Review E, Submitted.

Jin, G. (2006). Physics-Based Modeling of Sedimentary Rock Formation and Prediction of Transport Properties. PhD thesis, University of California, Berkeley, Berkeley, CA.

Krason, J., and M. Ciesnik, 1985, Geological Evolution and Analysis of Confrmed or Suspected

Krason, J., and P. D. Finley, 1992, Messoyakh Gas Field - Russia West Siberian Basin, TR: Structural Traps VII, AAPG, p. 197-220.

Lamb, T.W. & Whitman, R.V. (1979) *Soil Mechanics*. Wiley, New York, 553 pp.

Makogon, Y. F., 1974, Hydrates of natural gases, NEDRA, Moscow.

Makogon, Y. F., 1981, Hydrates of Natural Gas, PennWell.

Makogon, Y. F., 1984, Production from natural gas hydrate deposits: Gazovaya Promishlennost, v. 10, p. 24-26.

Makogon, Y. F., 1988, Natural gas hydrates - the state of study in the USSR and perspectives for its using, Third Chemical Congress of North America, Toronto, Canada.

Makogon, Y. F., 1997, Hydrates of hydrocarbons, PennWell, Tulsa.

Makogon, Y. F., 2007, Personal Communication.

Makogon, Y. F., S. A. Holditch, and T. Y. Makogon, 2005, Russian field illustrates gas-hydrate production: Oil and Gas Journal, v. 103, p. 43-47.

Makogon, Y. F., S. A. Holditch, and T. Y. Makogon, 2007, Natural gas hydrates - A potential energy source for the 21st century: Journal of Petroleum Science and Engineering, v. 56, p. 14-31.

Makogon, Y. F., F. A. Trebin, and A. A. Trofimuk, 1971a, Finding of a pool of gas in the hydrate state: DAN SSSR, v. 196, p. 197-206.

Makogon, Y. F., F. A. Trebin, A. A. Trofimuk, and N. V. Chersky, 1971b, Detection of a pool of natural gas in a solid hydrated state: Doklady Akademii Nauk SSSR, v. 196, p. 197-200.

Makogon, Y. F., V. P. Tsarev, and N. V. Chersky, 1970, Gas-hydrate resource in the offshore, 17th World Gas Congress, Moscow.

Meyerhoff, A. A., 1980, Petroleum basins of the Soviet Arctic: Geological Magazine, v. 117, p. 101-210.

Mindlin, R. D. (1949). Compliance of elastic bodies in contact. J. Appl. Mech., 16:259–268.

Mindlin, R. D. and Deresiewicz, H. (1953). Elastic spheres in contact under varying oblique forces. J. Appl. Mech., 20:327–344.

Moridis, G. J., and T. Collettt, 2003, Strategies for gas production from hydrate accumulations under various geologic conditions, Lawrence Berkeley National Laboratory.

Moridis, G. J., and T. Collettt, 2004, Gas production from Class 1 hydrate accumulations, *in* C.

Moridis, G. J., T. Collettt, S. R. Dallimore, T. Satoh, S. Hancock, and B. Weatherill, 2004, Numerical studies of gas production from several CH4 hydrate zones at the Mallik site, Mackenzie Delta, Canada: Journal of Petroleum Science and Engineering, v. 43, p. 219-238.

Moridis, G. J., and M. B. Kowalsky, 2005, Depressurization-induced gas production from class-1 hydrate deposits, SPE Annual Technical Conference and Exhibition, Dallas, Texas.

Moridis, G. J., M. B. Kowalsky, and K. Pruess, 2005, TOUGH-Fx/Hydrate v 1.0 User's Manual: A code for the simulation of system behavior in hydrate bearing geologic media.

Moridis, G. J., and E. D. Sloan, 2007, Gas production potential of disperse low-saturation hydrate accumulations in oceanic sediments: Energy Conversion and Management, v. 48, p. 1834-1849.

Sapir, M. H., E. N. Khramenkov, I. D. Yefremov, G. D. Ginsburg, A. E. Beniaminovich, S. M. lenda, and V. L. Kislova, 1973, Geologic and geophysical features of the gas hydrate deposits in the Messoiakh field: Geologiia Nefti i Gaza, v. 6, p. 26-34.

Sheshukov, N. L., 1973, Features of gas bearing strata with the hydrates: Geologiia Nefti i Gaza, v. 6, p. 20-26.

National Energy Technology Laboratory

626 Cochrans Mill Road
P.O. Box 10940
Pittsburgh, PA 15236-0940

3610 Collins Ferry Road
P.O. Box 880
Morgantown, WV 26507-0880

One West Third Street, Suite 1400
Tulsa, OK 74103-3519

1450 Queen Avenue SW
Albany, OR 97321-2198

2175 University Ave. South
Suite 201
Fairbanks, AK 99709

Visit the NETL website at:
www.netl.doe.gov

Customer Service:
1-800-553-7681